

1 **Novel ionic liquids-based extraction method that preserves molecular**  
2 **structure from cutin**

3  
4 *Carlos J.S. Moreira,<sup>a,±</sup> Artur Bento,<sup>a,±</sup> Joana Pais,<sup>a</sup> Johann Petit,<sup>b</sup> Rita Escórcio,<sup>a</sup> Vanessa G.*  
5 *Correia,<sup>a</sup> Ângela Pinheiro,<sup>a</sup>, Łukasz P. Haliński,<sup>c</sup> Oleksandr O. Mykhaylyk,<sup>d</sup> Christophe*  
6 *Rothan,<sup>b</sup> Cristina Silva Pereira<sup>a,\*</sup>*

7  
8 <sup>a</sup> Instituto de Tecnologia Química e Biológica António Xavier, Universidade Nova de Lisboa (ITQB NOVA), Av.  
9 da República, 2780-157, Oeiras, Portugal

10 <sup>b</sup> UMR 1332 BFP, INRAE, Univ. Bordeaux, F-33140 Villenave d'Ormon, France

11 <sup>c</sup> Department of Environmental Analysis, Faculty of Chemistry, University of Gdańsk, Wita Stwosza 63, 80-308  
12 Gdańsk, Poland

13 <sup>d</sup> Soft Matter Analytical Laboratory, Dainton Building, Department of Chemistry, The University of Sheffield,  
14 Sheffield, S3 7HF, UK

15 <sup>±</sup> equally contributing authors; \* corresponding author: Cristina Silva Pereira ([spereira@itqb.unl.pt](mailto:spereira@itqb.unl.pt))

16  
17 **Authors' contributions:** CSP supervised the project and the interpretation of data and prepared the final version of  
18 the manuscript. All authors have made substantial contributions to the acquisition, analysis and interpretation of data  
19 and contributed to the drafting of the manuscript: JP and CR (plant material preparation), CJSM, AB and RE (ionic  
20 liquid synthesis, cutin extraction and cryogenic milling), AB, VGC (NMR data analysis); JP, AP, JP and LH (GC-  
21 MS analyses); OOM and AB (WAXS analyses), AB and CJSM (DSC analyses); CJSM and AB (preparation of the  
22 initial draft of the manuscript). All authors read and approved the final version of the manuscript.

23  
24

## 25 **Abstract**

26 The biopolyester cutin is ubiquitous in land plants, building the polymeric matrix of the plant's  
27 outermost defensive barrier - the cuticle. Cutin influences many biological processes *in planta*  
28 however due to its complexity and highly branched nature, the native structure remains partially  
29 unresolved. Our aim was to define an original workflow for the purification and systematic  
30 characterisation of the molecular structure of cutin. To purify cutin we tested the ionic liquids  
31 cholinium hexanoate and 1-butyl-3-methyl-imidazolium acetate. The ensuing polymers are  
32 highly esterified, amorphous and have the typical monomeric composition as demonstrated by  
33 solid state NMR, complemented by spectroscopic (GC-MS), thermal (DSC) and x-ray scattering  
34 (WAXS) analyses. A systematic study by solution-state NMR of cryogenically milled cutins  
35 extracted from Micro-Tom tomatoes (the wild type and the *gpat6* and *cus1* mutants) was  
36 undertaken. Their molecular structures, relative distribution of ester aliphatics, free acid end-  
37 groups and free hydroxyl groups, differentiating between those derived from primary and  
38 secondary esters, were solved. The acquired data demonstrate the existence of free hydroxyl  
39 groups in cutin and reveal novel insights on how the mutations impact the esterification  
40 arrangement of cutin. Compared to conventional approaches, the usage of ionic liquids for the  
41 study of plant polyesters opens new avenues since simple modifications can be applied to  
42 recover a biopolymer carrying distinct types/degrees of modifications (*e.g.* preservation of esters  
43 or cuticular polysaccharides), which in combination with the solution NMR methodologies  
44 developed here, constitutes now essential tools to fingerprint the multi-functionality and the  
45 structure of cutin *in planta*.

46

## 47 **Introduction**

48 Plant polyesters, namely cutin and suberin, are the third most abundant plant polymers right after  
49 cellulose/hemicellulose and lignin. Naturally, due to their high abundance in nature, plant  
50 polyesters are considered as promising substitutes to petroleum-based plastics (Heredia-Guerrero  
51 et al., 2017). In particular, cutin makes up the polymeric matrix of the cuticle that builds the  
52 protective layer of the aerial parts of land plants; an evolutionary feature acquired during the  
53 colonization of terrestrial environments (Fich et al., 2016). The cuticle constituents (cutin and  
54 waxes) are deposited onto the polysaccharide layer of the walls of the epidermal cells (Segado et

55 al., 2016). Cutin is, in general, a highly branched polymer, mainly composed of C16 and C18  
56 fatty acids, containing mostly terminal ( $\omega$ -hydroxyl) and *mid*-chain hydroxyl group, linked  
57 through ester bonds. Other functional groups such as aromatics, dicarboxylic acids and glycerol  
58 can also be found in cutin at low amounts (Mazurek et al., 2017).

59 Over the years, many authors have contributed to elucidate the roles played by cutin in  
60 diverse biological processes along plant development, growth and response to biotic and/or  
61 abiotic stresses (Fich et al., 2016). However, current methods for the extraction and analysis of  
62 cutin polyesters have inherent limitations. The extraction of cutin from a plant source usually  
63 relies on time-consuming processes that include enzymatic digestion of polysaccharides followed  
64 by thorough organic solvent extraction of the soluble waxes present in the cuticle (Chatterjee et  
65 al., 2012). In addition, the most frequent chemical analysis of cutin are based on total/partial  
66 hydrolyses of the polyesters and therefore disclose solely the monomeric constituents attained  
67 through (Graça and Lamosa, 2010; Fernández et al., 2016), regardless that sometimes solid state  
68 spectroscopic based analyses of the polymer are also used (Deshmukh et al., 2003; Fernández et  
69 al., 2016). The monomeric constituents can disclose a partial view of the basic composition of  
70 the biopolymer (*i.e.* of the hydrolysable constituents), while providing insights on its  
71 biosynthesis (Bakan and Marion, 2017) but not of their supra-molecular organisation, which  
72 remains largely unknown (Fich et al., 2016; Bakan and Marion, 2017). To advance our  
73 understanding of important cutin-related questions such as cutin/cell wall polymers interactions  
74 or the role of cutin in defence to pathogens (Chatterjee et al., 2016), a better insight into the  
75 structure of cutin in its native state is highly required.

76 Ionic liquids – usually defined as salts on a liquid state below 100 °C – may facilitate the  
77 processing of plant polymers due to their capacity to induce swelling/solubilisation and/or to  
78 catalyse the cleavage of specific inter-molecular bonds (Rogers and Seddon, 2003). In particular,  
79 some imidazolium-based ionic liquids can efficiently disrupt the intermolecular hydrogen  
80 bonding between hydroxyl groups in cellulose (Li et al., 2018) whereas some cholinium  
81 alkanoates can catalyse selectively the hydrolysis of inter-molecular acylglycerol esters (Garcia  
82 et al., 2010; Ferreira et al., 2012; Ferreira et al., 2014). The latter ionic liquid was used by us to  
83 extract suberin from cork – a plant polyester sharing chemical similarities with cutin – by  
84 catalysing a selective and mild hydrolysis of acyl glycerol esters yet preserving most extant  
85 linear aliphatic esters (Ferreira et al., 2014; Correia et al., 2020).

86           Our aim was to establish a novel cutin extraction method that allows the study of native  
87 cutin architecture and properties and is applicable to a wide range of plant species and tissues. To  
88 meet these criteria, the newly-developed method should be easy to process and rapid and should  
89 preserve the chemical structure of the cutin. To this end, we first established an ionic liquid  
90 approach for the extraction of cutin, with the solubilisation of cutin from tomato peel as a proof-  
91 of-concept. We demonstrated that the cholinium hexanoate process renders a near native cutin as  
92 shown by Scanning Electronic Microscopy (SEM), <sup>13</sup>C Magic Angle Spinning Nuclear Magnetic  
93 Resonance (<sup>13</sup>C MAS NMR), and Differential Scanning Calorimetry (DSC) analyses of the cutin  
94 structure. These analyses were complemented by Gas Chromatography – Mass Spectrometry  
95 (GC-MS) analyses of the hydrolysable constituents. In addition, we established for the first time  
96 the molecular structure in solution of near native cutins (solubilised with the aid of cryogenic  
97 milling) through high-resolution one- and two-dimensional solution state NMR analyses.  
98 Extension of our approach from a processing tomato cultivar to the miniature Micro-Tom  
99 cultivar, including two cutin biosynthesis and polymerisation mutants, highlighted the  
100 consistency of our findings with published results but also revealed new features of near native  
101 cutin. We therefore believe that our methodological approach will support discovery in the field  
102 of cutin biogenesis and biosynthesis.

103

104

## 105 **Results**

### 106 **A highly esterified cutin was purified using ionic liquids that mediate mostly the dissolution** 107 **of sub-cuticular polysaccharides**

108 Seeking to establish a novel methodology to extract cutin from tomato peels, we resorted to  
109 cholinium hexanoate and 1-butyl-3-methyl-imidazolium acetate (hereafter defined as BMIM  
110 acetate). Cholinium hexanoate was chosen because of its ability to mediate the extraction of  
111 suberin from cork through mild and selective hydrolysis of acylglycerol ester bonds (Ferreira et  
112 al., 2014), and BMIM acetate due to its proven ability to mediate the dissolution of cellulose (Li  
113 et al., 2018). First, we tested if either ionic liquid (100 °C without stirring) hydrolyses glyceryl  
114 trioctanoate and octyl octanoate that contain an acylglycerol ester bond and a linear aliphatic  
115 ester bond, respectively. Glyceryl trioctanoate was hydrolysed in the presence of both ionic  
116 liquids, yet the efficiency of the reaction was higher when cholinium hexanoate was used (Fig.  
117 1). Cholinium hexanoate did not catalyse the cleavage of octyl octanoate (Fig. 1A), contrary to  
118 the BMIM acetate that catalysed this reaction though inefficiently (Fig. 1B). As previously  
119 reported, cholinium hexanoate catalyses specifically the hydrolysis of acylglycerol esters  
120 (Ferreira et al., 2014), regardless that in the present study the absence of agitation and the higher  
121 water content of the ionic liquid reduced the reaction efficiency.

122 We then tested the potential of these ionic liquids for the isolation of cutin from tomato  
123 peels after 2, 15 and 170 hours compared to a conventional method (*i.e.* enzymatic removal of  
124 polysaccharides followed by organic solvent mediated dewaxing). In the process of suberin  
125 extraction from cork using cholinium hexanoate, suberin in the filtrate is recovered by  
126 precipitation in an excess of water (Ferreira et al., 2012). We preliminarily tested a 2 hours  
127 reaction of cutin peels in cholinium hexanoate, and verified using ATR-FTIR that the archetypal  
128 bands assigned to cutin, *i.e.* long chain aliphatics (CH<sub>2</sub> and C=O), were detected in the insoluble  
129 fraction (not in the filtrate as observed for cork suberin) whereas the filtrate shows enrichment in  
130 bands usually assigned to polysaccharides (C-O-C) (Supplementary Fig. S1). Accordingly, the  
131 produced insoluble fractions were characterised using SEM (Fig. 2) and <sup>13</sup>C MAS NMR (Fig.  
132 3A). SEM imaging of the cutins extracted with either ionic liquid are virtually identical: a clean  
133 thick cutin-continuum showing the epidermal cells grooves (Fig. 2A-F). In the reference cutin,  
134 *i.e.* obtained through the conventional enzymatic-based process, the cutin-continuum apparently  
135 overlaps with other cellular components, and many intracellular spaces are not hollow (Fig. 2G).

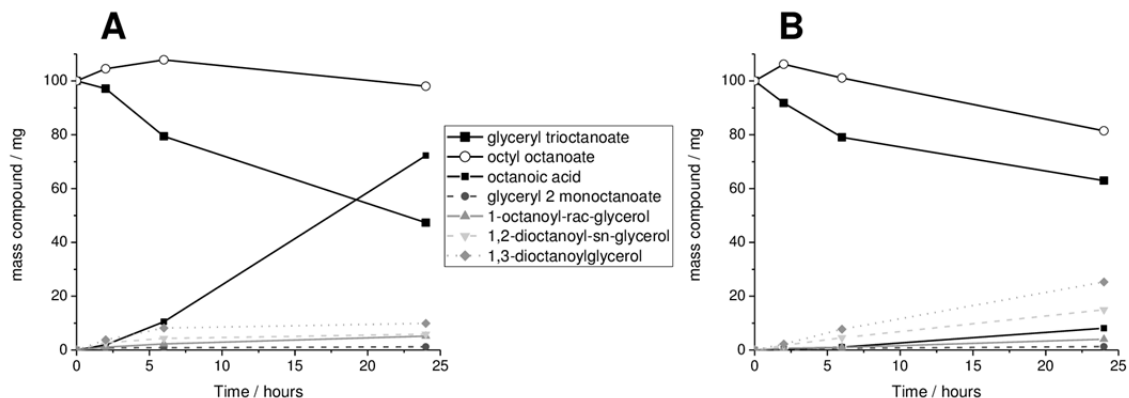


**Fig. 1.** Compounds detected after the reaction of glyceryl trioctanoate and octyl octanoate with either cholinium hexanoate (A) or 1-butyl-3-methylimidazolium acetate (B) for 2, 6 and 24 hours (the observed average standard errors were negligible, < 4%). All compounds were identified and quantified by GC-MS. At time zero, glyceryl trioctanoate and octyl octanoate were assumed to represent the only compounds present in mixture.

136 In the  $^{13}\text{C}$  MAS NMR spectrum of the reference cutin, the major structural classes  
137 assigned to cutin include the long methylene chains -  $(\text{CH}_2)_n$  with major peaks at 26, 29 &  
138 34 ppm, the oxygenated aliphatics -  $\text{CH}_2\text{O}$  (63 ppm) and  $\text{CHO}$  (73 ppm), and the carboxyl  
139 groups at 172 ppm, comprising the contribution of both esters and acids (Chatterjee et al., 2016)

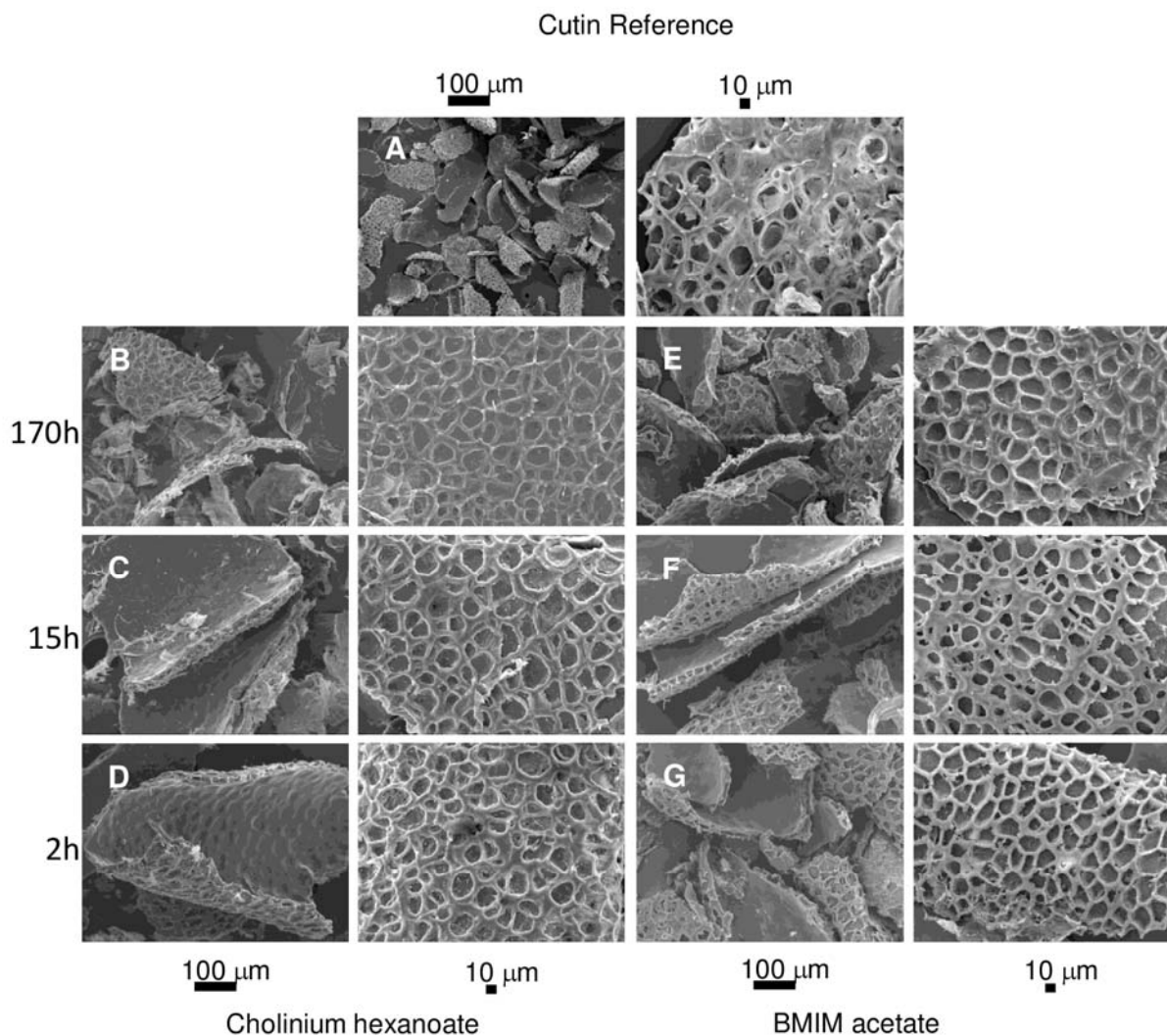


**Fig. 2.** SEM imaging of cutin purified after treatment with cholinium hexanoate (B-D) or 1-butyl-3-methylimidazolium acetate (E-G) after 2, 15 and 170 hours. All samples show a clean thick cutin-continuum comprising the epidermal cells grooves. A representative cutin reference sample (*i.e.* obtained through the conventional enzymatic-based process) is also shown denoting many intracellular spaces that are not hollow (A).

140 (Fig. 3A). Only minor signals can be assigned to the aromatic region (105 & 130 ppm). The  
141 spectral signatures of the remaining cutins are very similar regardless of used ionic liquid and  
142 extraction time and also similar to the reference cutin spectrum (Fig. 3 and Table 1). The relative  
143 contributions of the signals assigned to aromatics for the cutins purified with either ionic liquid

144 increased along the reaction time, possibly an artefact derived from phase corrections. The  
145 relative contributions of the oxygenated aliphatics region (57-92 ppm) are higher in the ionic  
146 liquid extracted cutins compared to the reference cutin (Fig. 3A). This region might also  
147 comprise resonances derived from polysaccharides (Chatterjee et al., 2016). Most subcuticular  
148 polysaccharides can be removed from cutin using an acidic hydrolysis mediated by TFA  
149 (Arrieta-Baez and Stark, 2006), regardless that cellulose might not be totally removed  
150 (Hernández Velasco et al., 2017). In the present study, the NMR spectra of cutins obtained using



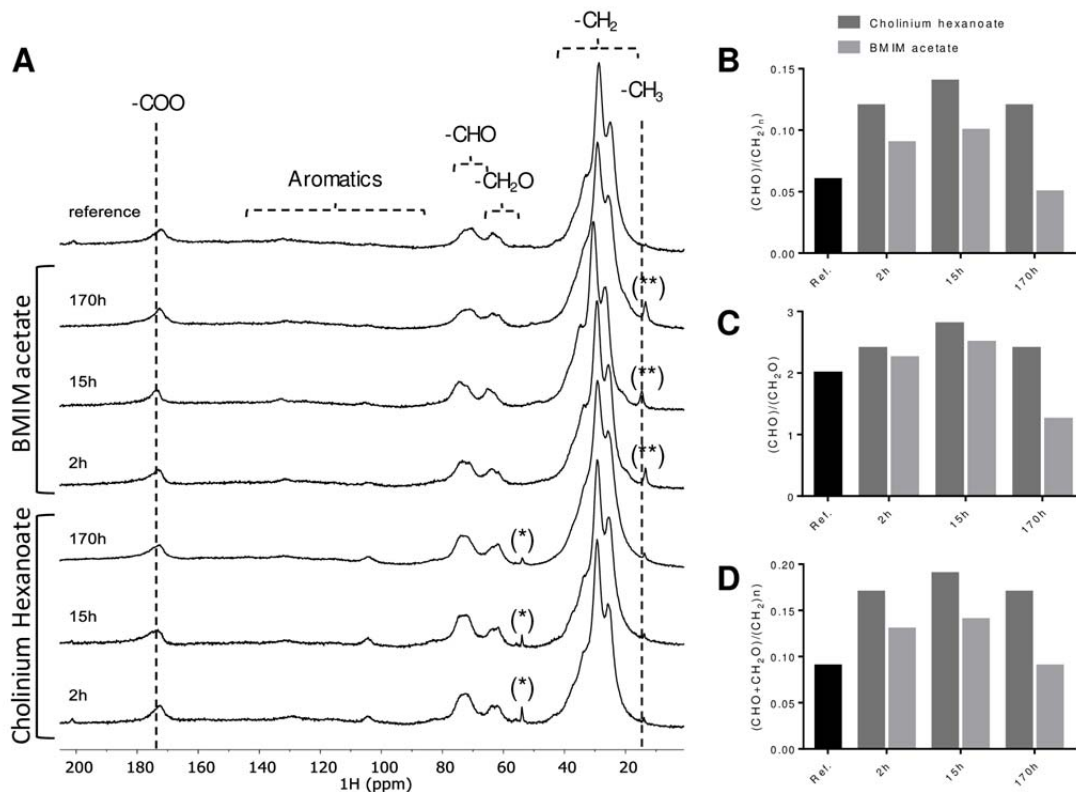


**Fig. 3.**  $^{13}\text{C}$  MAS NMR spectra obtained for the cutin reference and the cutin samples derived from reactions with cholinium hexanoate or 1-butyl-3-methylimidazolium acetate after 2, 15 and 170 hours (A) and the corresponding calculated reticulation (B-C) and esterification (D) ratios. The regions assigned to the long methylene chains, the oxygenated aliphatics, aromatics and the carboxyl groups are marked. The imidazolium-based cation contributes to the signal assigned to the CH<sub>3</sub> groups (15 ppm \*\*), whereas the cholinium cation is seen in the signal at 54 ppm \*; both contaminants can be washed out.

151 the cholinium hexanoate (2 h reaction) before and after the acidic hydrolysis treatment are  
 152 virtually identical (Table 1, Supplementary Fig. S2). The few observed alterations can be  
 153 explained by the hydrolysis of esters during the acidic treatment (Arrieta-Baez and Stark, 2006).  
 154 Based on these results, the oxygenated aliphatics region can be mostly assigned to cutin.  
 155 Consequently, the biopolymer reticulation level can be reasonably estimated through the ratio of  
 156 signal's integral in the CHO region of the oxygenated aliphatics (67-92 ppm) with that of the  
 157 entire aliphatic region (8-50 ppm) or that of the CH<sub>2</sub>O region (57-67 ppm) (Matas et al., 2011;

158 Chatterjee et al., 2016). Based on the calculated reticulation ratios, cholinium hexanoate usage  
159 apparently rendered a biopolymer displaying higher reticulation compared to either that attained  
160 with the BMIM acetate or the conventional approach (Fig. 3B-C). At this stage, one cannot  
161 exclude that the presence of cellulose embedded in the biopolymer might increase the estimated  
162 reticulation levels. A similar trend was observed when estimating their esterification levels (Fig.  
163 3D), which can be inferred through the ratio between the integral of the total oxygenated  
164 aliphatic region (CHO & CH<sub>2</sub>O) with that of the entire aliphatic region (8-50 ppm) (Matas et al.,  
165 2011). The esterification of the cholinium cation with cutin's free acids was reported before as  
166 mechanistically very unlikely (Ferreira et al., 2014).

167 In order to further elucidate if the ionic liquid-based extractions can indeed render a near  
168 native-cutin we resorted to DSC (Fig. 4A) and WAXS (Fig. 4B) measurements of the cutins  
169 extracted with the ionic liquids (2 and 170 hours) together with the reference cutin. The DSC  
170 thermograms are depicted in Fig. 4A. The cutins extracted using either ionic liquid for 2 hours  
171 show higher enthalpy energies for melting the biopolymer and lower melting temperatures  
172 ( $\Delta H=129.6 \text{ J}\cdot\text{g}^{-1}$  &  $T_m = 100.5 \text{ }^\circ\text{C}$  and  $\Delta H=97.5 \text{ J}\cdot\text{g}^{-1}$  &  $T_m = 100.6^\circ\text{C}$ , for cholinium hexanoate  
173 and BMIM acetate, respectively) compared to the reference cutin ( $\Delta H=70.5 \text{ J}\cdot\text{g}^{-1}$  &  
174  $T_m = 114.5 \text{ }^\circ\text{C}$ ). All thermograms show a relatively broad melting curve (Fig. 4A), which is  
175 typical for heterogeneous and amorphous materials (Benítez et al., 2018) and similar glass  
176 transition temperatures (ca.  $-20 \text{ }^\circ\text{C}$ ). The peaks for the cutins which originated from the 2 hours  
177 ionic liquid reactions are less broad compared to the reference cutin, suggestive of increased  
178 homogeneity. This feature was lost when extensive reaction times were used, consistent with the  
179 estimated reduction in the biopolymer reticulation and esterification (Fig. 3B-D). The WAXS  
180 patterns of all cutin samples (Fig. 4B) are mainly represented by a broad diffuse peak with the  
181 maximum intensity at  $q \sim 1.41 \text{ \AA}^{-1}$  which most likely corresponds to an amorphous structure  
182 commonly formed by organic polymeric materials with an inter-chain distance of around  $4.5 \text{ \AA}$ .  
183 Considering cutin's composition, this amorphous structure should be related to randomly-packed  
184 acyl chains. In contrast to the reference cutin, the scattering patterns of cutins extracted by either  
185 ionic liquid show diffraction peaks indicating the presence of a crystalline component. The first  
186 diffraction peak at  $q = 1.52 \text{ \AA}^{-1}$  and the second peak at  $q = 1.69 \text{ \AA}^{-1}$ , noticeable for the cutin  
187 extracted by cholinium hexanoate for 170 h (Fig. 4A, blue curve), can be assigned to an  
188 orthorhombic crystal structure (space group Pnma, Miller indexes 110 and 200, respectively)

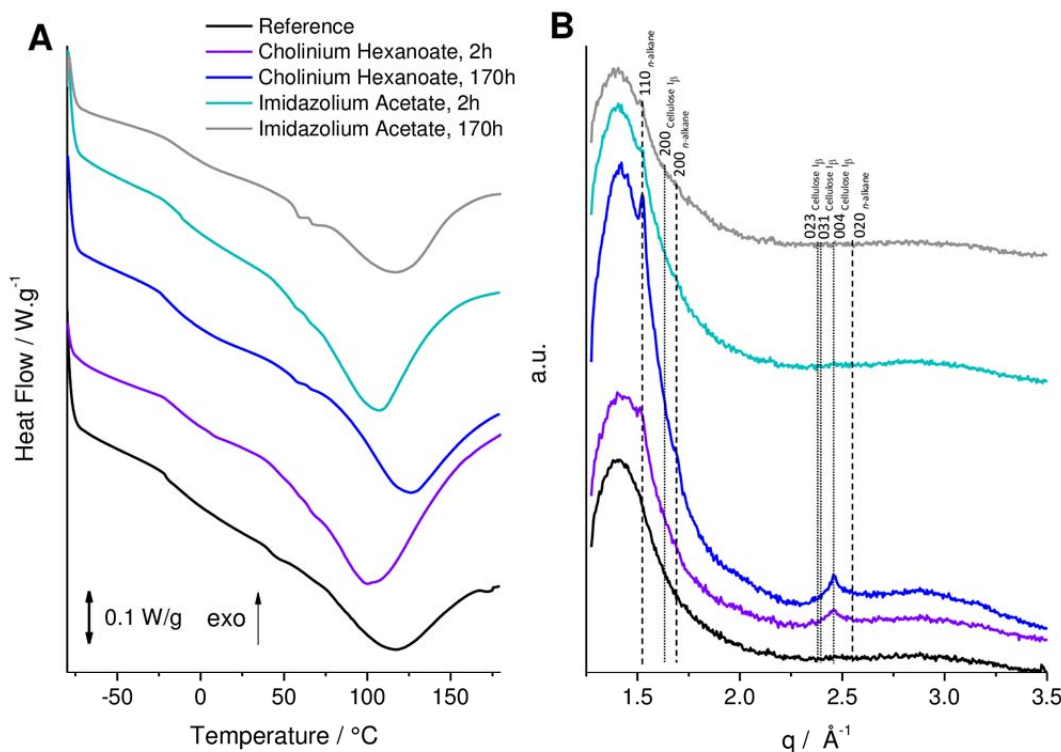


**Fig. 4.** DSC thermograms (A) and WAXS patterns (B) collected for a reference enzymatically-extracted cutin (black curve) and cutin powders extracted from tomato peels using ionic liquids for various durations of the treatment [cholinium hexanoate (purple curve for 2 hours and blue curve for 170 hours) and imidazolium acetate (cyan curve for 2 hours and grey curve for 170 hours)]. The vertical straight lines in WAXS patterns indicate position of diffraction peaks of cellulose (dotted lines) and crystallised *n*-alkane chains (dashed lines). Miller indexes assigned to the lines correspond to cellulose I<sub>β</sub> (monoclinic space group P12<sub>1</sub>1) and *n*-alkane chain packing (orthorhombic space group Pnma).

189 commonly formed by compounds comprised of alkane-like chains such as triacylglycerols (b'  
 190 phase) (Mykhaylyk et al., 2007) or polyethylene (Bunn, 1944; Southern et al., 1972). This  
 191 suggests that the extraction of cutin by the ionic liquids enriches this material with a crystalline  
 192 component where some acyl chains tend to form crystals. A low level of branching of acyl  
 193 chains in cutin possibly is favourable for the formation of an orthorhombic unit cell, which is  
 194 thermodynamically more stable than the rotator phase formed by distorted alkane chains packed

195 in a hexagonal array (Small, 1984). This observation is consistent with the DSC measurements  
196 (Fig. 4A) indicating that the cutin extracted by cholinium hexanoate for 170 h, containing the  
197 highest fraction of the acyl crystalline component, has the highest peak melting point. The third  
198 diffraction peak at  $q = 2.46 \text{ \AA}^{-1}$ , observed for cutin extracted by cholinium hexanoate (Fig. 4B,  
199 purple and blue curves), cannot be related to the acyl chain crystalline structure. Its position is  
200 significantly shifted from a possible 020 peak at  $q = 2.55 \text{ \AA}^{-1}$  generated by the orthorhombic  
201 structure (Fig. 4B). The third peak is likely to be associated with a crystalline cellulose and can  
202 be assigned to 004 reflection of monoclinic cellulose  $I_{\beta}$  (space group  $P12_11$ ) (Rongpipi et al.,  
203 2019). It has to be noted that the most intense 200 diffraction peak of the cellulose  $I_{\beta}$  expected at  
204  $q = 1.63 \text{ \AA}^{-1}$  is not visible because of an overlap with the intense broad peak corresponding to the  
205 amorphous structure. Crystalline cellulose usually coexists with amorphous cellulose (Rongpipi  
206 et al., 2019). However, it would be difficult, if possible at all, to identify the cellulose amorphous  
207 component with its expected peak maximum intensity at  $q = 1.52 \text{ \AA}^{-1}$  from the broad diffuse  
208 peak observed by WAXS. Neither enzymatically-extracted cutin (reference cutin) nor cutin  
209 extracted by BMIM acetate reveal the presence of crystalline cellulose in their scattering patterns  
210 (Fig. 4B, black, cyan and grey curves), indicating that both extraction methods led to its  
211 successful removal. This observation together with the higher relative contribution of the  
212 oxygenated aliphatics region for the cutin extracted with BMIM acetate compared with the  
213 reference cutin (Table 1) suggests that some oxygenated aliphatics are lost during the enzymatic  
214 treatment.

215 Finally, the relative abundances of hydrolysable cutin constituents were determined by  
216 GC-MS to disclose how the ionic liquid extraction methods influence the composition of the  
217 biopolymer compared to the reference method (Table 2, Supplementary Fig. S3). The reference  
218 cutin comprises *ca.* 13% of non-hydrolysable constituents, whereas those attained with an ionic  
219 liquid display significantly higher recalcitrance (*ca.* 20% to 30%), consistent with their estimated  
220 higher reticulation (Fig. 3B-C). In general, the monomeric compositions of the ionic liquid  
221 extracted cutins are similar to that of the cutin reference (and also to the starting material) (Table  
222 2). Both the abundance and the diversity of fatty acids, decreased as the reaction time in the ionic  
223 liquid increased (Table 2). This was more pronounced when BMIM acetate was used for 170  
224 hours, which rendered a cutin that is almost devoid of fatty acids and also containing nearly two  
225 times less dicarboxylic acids. The fatty acids carry a methyl end-group that is esterified to the

226 biopolymer through a single bond. After 170 hours of reaction in BMIM acetate, the amount of  
227 10,16-dihydroxyhexadecanoic acid that was lost from the biopolymer (*i.e.* solubilised) was  
228 nearly threefold higher than when cholinium hexanoate was used (data not shown).

### 229 **A snap-shot of the molecular structure of cutin purified by cholinium hexanoate reveals** 230 **extant free hydroxyls and free acids**

231 Our data made evident the potential of using short time reactions with either ionic liquid to  
232 recover from tomato peels a cutin continuum displaying esterification/reticulation levels and  
233 composition near to that found *in planta*. In addition, cholinium hexanoate presents several  
234 advantages compared to the BMIM acetate. It cleaves fewer esters bonds, rendering a more  
235 esterified biopolymer (Fig. 3d), and contrary to the BMIM acetate, it is also biocompatible and  
236 biodegradable (Petkovic et al., 2010).

237 Recently, we resolved the molecular structure of *in situ* suberin using solution state  
238 NMR, upon its solubilisation in heated DMSO directly from cork after four hours of cryogenic  
239 milling (Correia et al., 2020). This inspired us to apply cryogenic milling for the solubilisation of  
240 a cutin extracted with cholinium hexanoate after two hours. Solving cutin's molecular structure  
241 would create conditions to look "inside" its backbone, specifically to its esterification  
242 arrangement. The GC-MS analyses disclosed only the composing hydrolysable constituents  
243 (Table 2) and the solid-state analyses –  $^{13}\text{C}$  MAS NMR, DSC and WAXS (Fig. 3 and 4) –  
244 revealed only the bulky chemical functionalities and properties of the purified cutins. Only after  
245 10 hours of cryogenic milling the cutin was solubilised in DMSO, reflecting cutin's much lower  
246 solubility compared to suberin. We analysed the impact of the cryogenic milling process,  
247 especially the occurrence of oxidation reactions inside the grinding jar due to possible  
248 condensation of oxygen at low temperatures. Elemental analysis of cutin before and after the  
249 cryogenic milling process, revealed that the relative percentage of the tested elements, including  
250 oxygen (Supplementary Table S2), were unaltered after the treatment. Therefore, despite this  
251 solubility drawback, for the first time, a solution state  $^1\text{H}$  NMR could be acquired with good  
252 resolution showing the presence of many overlapping signals (Fig. 5A); an archetypal feature  
253 observed in other complex multifunctional polymers (Lyerla, 1980). The relative abundances of  
254 aliphatics,  $\text{CH}/\text{CH}_2\text{-X}$  oxygenated aliphatics and aromatics were estimated through the  
255 integration of the  $^1\text{H}$ -spectrum as 70%, 27% and 3%, respectively. The assignment of  $^1\text{H}$   
256 chemical shifts for the constituent monomers was then achieved through a combination of  $^1\text{H}$ - $^1\text{H}$

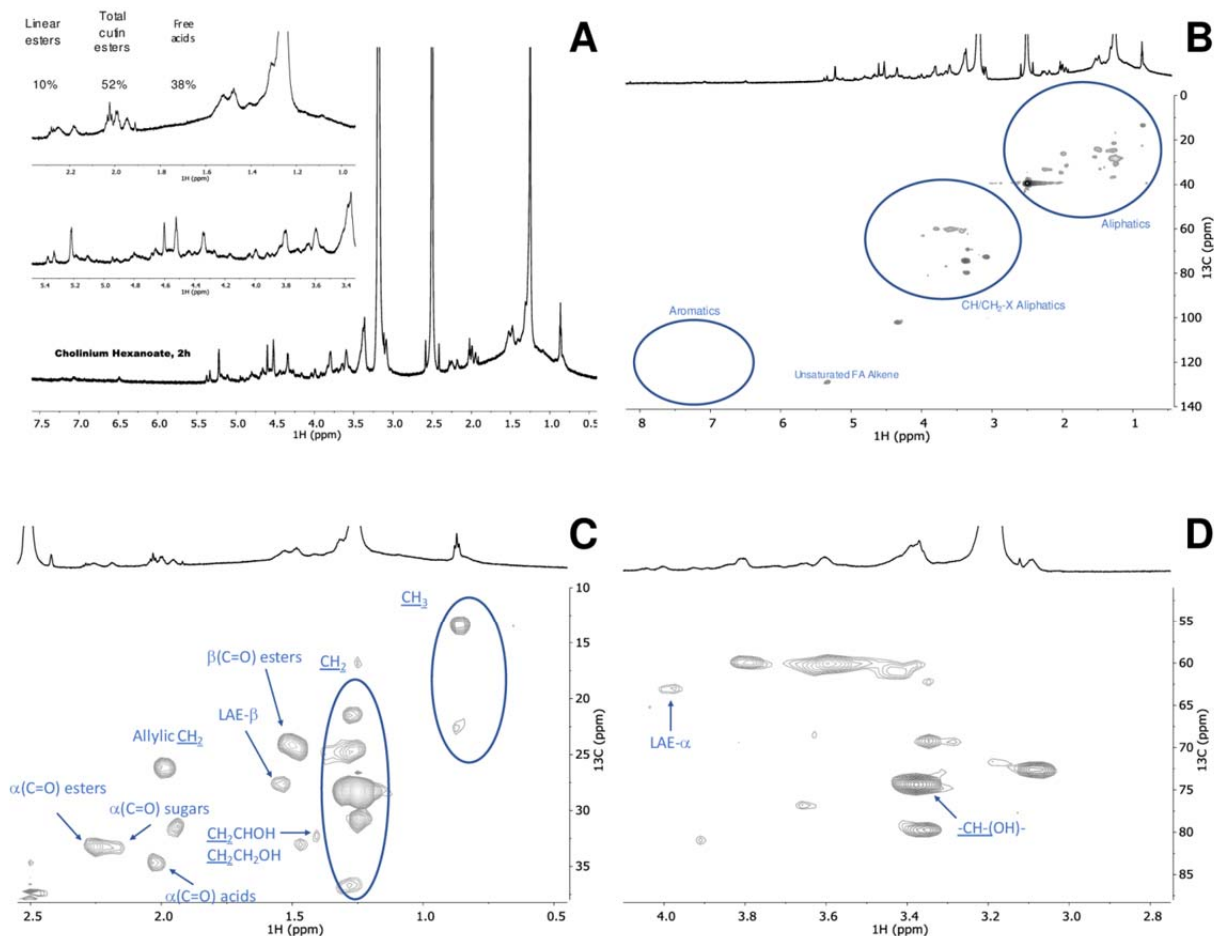


**Fig. 5.** Wide-ranging NMR spectral characterisation of cutin isolated with cholinium hexanoate (2 h). The  $^1\text{H}$  NMR, with inserts focussing the aliphatic and oxygenated aliphatics regions (A); and the HSQC spectrum: full (B) and regions corresponding to aliphatics (C) and CH/CH<sub>2</sub>-X aliphatics (D) of the purified cutin. Some correlations (unlabelled) are uncertain or unidentified.

257 (COSY) and  $^1\text{H}$ - $^{13}\text{C}$  (HSQC, HMBC) correlation experiments (Supplementary Fig. S4 to S7).  
 258 Previous NMR-based data of tomato cutin were attained through solution state NMR analyses of  
 259 oligomeric structures obtained by methanolysis of tomato peels (Graça and Lamosa, 2010) and  
 260 through HR-MAS NMR analyses of the tomato cutin swelled in DMSO (Deshmukh et al., 2003).  
 261 These studies provided important baseline information for the assignment of the spectrum of  
 262 cutin extracted with cholinium hexanoate for two hours (Supplementary Table S2).

263 The full range HSQC spectrum of cutin is depicted in Fig. 5B, highlighting the regions  
 264 corresponding to aliphatics and CH/CH<sub>2</sub>-X aliphatics as well as aromatics. A detailed analysis of

265 the HSQC spectrum of the two aliphatics regions with the assignment of CH<sub>2</sub> and CH<sub>3</sub> groups  
266 from the aliphatic chains, the ester bonds and the free mid-chain hydroxyl groups is shown in  
267 Fig. 5C-D. Only secondary free hydroxyl groups were visible in the HSQC spectrum (CHOH  
268 *mid-chain*), consistent with their presence in cutin as suggested before (Philippe et al., 2016).  
269 This observation is in agreement with the demonstration that cholinium hexanoate does not  
270 cleave primary esters bonds (Fig. 1). Here we assigned the β-(C=O) esters to a <sup>1</sup>H shift of 1.49  
271 ppm and <sup>13</sup>C shift of 24 ppm but we could not detect the signal of β-(C=O) acids, regardless that  
272 they have been assigned before in tomato cutin using HR-MAS NMR (Deshmukh et al., 2003).  
273 Deshmukh *et al.* (2003) assigned the signals of aliphatic esters, primary and secondary alcohols,  
274 free acids and α-branched carboxylic acids, yet the last two assignments could not be confirmed  
275 by HMBC. In the present study, the signals of the β-(C=O) acids possibly overlap with that of  
276 the esters and their differentiation from the small chemical shift differences observed in the  
277 acquired HSQC is virtually impossible. The signal α-(C=O) display two <sup>1</sup>H signals with a <sup>13</sup>C  
278 shift of 33 ppm, namely at 2.25 ppm and 2.19 ppm, which can be assigned to esters and acids,  
279 respectively. The α-(C=O) signal with a <sup>1</sup>H shift of 2.17 ppm has been previously assigned to  
280 xylan esters (Zhang et al., 2016). Based on the detection of vestigial amounts of microcrystalline  
281 cellulose in the cutin extracted with cholinium hexanoate for 2 hours (Fig. 4B), this signal may  
282 be associated to the presence of cellulose esters. Analysis of the cutin extracted with BMIM  
283 acetate (upon its cryogenic milling), which is apparently devoid of microcrystalline cellulose  
284 (Fig. 4B), showed that the signal α-(C=O) display a <sup>13</sup>C shift of 33 ppm and only a <sup>1</sup>H shift of  
285 2.26 ppm (Supplementary Fig. S6). Finally, to precisely assign the free acids in the cutin  
286 extracted with cholinium hexanoate for 2 hours, we acquired the HMBC spectrum that confirmed  
287 their signal at a <sup>13</sup>C shift of 35 ppm and a <sup>1</sup>H shift of 2.02 ppm (Supplementary Fig. S7). This  
288 observation is consistent with that previously assigned in cork suberin where the signal of the  
289 acid is at a <sup>13</sup>C shift of 36 ppm and a <sup>1</sup>H shift of 2.03 ppm, and that of the esters displays a <sup>13</sup>C  
290 shift of 34 ppm and a <sup>1</sup>H broad shift from 2.33-2.27 ppm (Correia et al., 2020).

291 Based on the assignments defined above, we calculated through integration of the signals  
292 in the <sup>1</sup>H NMR the relative abundance of free acids, of total esters (comprising primary and  
293 secondary aliphatic esters yet excluding sugar esters) and of linear esters as 38%, 52% and 10%,  
294 respectively (Fig. 5A, *see text-insert*). No acylglycerol bonds were detected in the HSQC  
295 analyses of cutin (Fig. 5B), consistent with the very low abundance of glycerol in tomato cutin

296 (Fich et al., 2016). We hypothesise that the free acids detected in the cutin spectra might mostly  
297 account for their natural occurrence, though one cannot exclude, at this stage, that some aliphatic  
298 esters might underwent cleavage in the presence of cholinium hexanoate.

299 **Ionic liquid extraction followed by solution NMR as a new tool to scrutinise the impact of**  
300 **specific mutations in the molecular structure of cutin from Micro-Tom tomatoes**

301 Solving the molecular structure in solution of a near native cutin isolated from a processing  
302 tomato cultivar, challenged us to test the suitability of the established cholinium hexanoate  
303 extraction for two hours, for the purification and systematic characterisation of cutins isolated  
304 from the tomato miniature cultivar Micro-Tom particularly well-suited for laboratory studies  
305 (Just et al., 2013; Garcia et al., 2016). To introduce known diversity in native cutin composition  
306 and structure, we further used both the wild type and the *gpat6* (*GLYCEROL-3-PHOSPHATE*  
307 *ACYLTRANSFERASE* gene) and the *cus1* (*CUTIN SYNTHASE* gene) (Petit et al., 2016; Philippe  
308 et al., 2016; Petit et al., 2017) mutants that show phenotypes with altered cutin composition and  
309 altered degree of intra-chain branching. In particular, in the *gpat6* mutant (formerly named cutin-  
310 deficient mutant *cut1*; (Philippe et al., 2016)) the synthesis of the major cutin precursor is  
311 hampered, hence a thinner cuticle is produced with overall decreased levels of cutin, which is  
312 enriched in fatty acids (Petit et al., 2016). In contrast, in the *cus1* tomato mutants, cutin  
313 polymerization is impaired (Girard et al., 2012; Yeats et al., 2012) and the esterification of  
314 secondary OH groups of the dihydroxy acids is significantly reduced (Philippe et al., 2016). To  
315 minimize any possible effect of the environmental conditions on the expression of the fruit  
316 cuticle phenotype, the *gpat6* and *cus1* mutants were grown side-by-side with wild type plants.  
317 The relative abundance of the hydrolysable constituents in the Micro-Tom cutins purified with  
318 cholinium hexanoate is depicted in Table 3. In general, the observed diversity/abundances of  
319 hydrolysable constituents are similar to that previously reported (Petit et al., 2016; Philippe et al.,  
320 2016), regardless of some variations, possibly due to disparities in tomato growth conditions in  
321 the greenhouse (season, light, temperature and hygrometry). In addition, the cutins which  
322 originated from the mutants show an increase in the relative abundance of non-hydrolysable  
323 constituents compared to the wild type (*ca.* 10% increase), and their identification yields  
324 decreased nearly 20% due to higher diversity of unidentified monomers (Table 3). Cutin from  
325 both mutants display higher relative abundance of fatty acids and dicarboxylic acids (nearly



326 tenfold and twofold, respectively) and lower of  $\omega$ -hydroxyacids (five to three times) compared to  
327 the wild type cutin.

328 To confirm that free acids naturally occur in cutin (hence differentiating these from free  
329 acid groups formed during the ionic liquid extraction), we compared the spectrum of cutin from  
330 the wild-type cultivar purified by the ionic liquid with that of the solubilised cuticle *via*  
331 cryogenic milling (Fig. 6). The obtained  $^1\text{H}$  NMR (Fig. 6A-B) and HSQC spectra (Fig. 6 C-F)  
332 are very similar, regardless that the presence of non-cutin constituents in the cuticle contributes  
333 to the appearance of many new signals, yet to be assigned, *e.g.* in the  $\text{CH}_3$  region (Fig. 6D).  
334 Importantly, the signals previously assigned to free acids –  $\alpha$ -(C=O) acids – are visible in both  
335 samples (Fig. 6C-D), which were confirmed in the corresponding HMBC spectra  
336 (Supplementary Fig. S10). Accordingly, the free acids detected in the ionic liquid purified cutins  
337 (Fig. 5A-C and 6A-B) reflect their natural presence. The signal attributed to the terminal  
338 hydroxyls was only detected in the spectrum of the ionic liquid extracted Micro-Tom cutin (Fig.  
339 6E). This observation suggests that the cholinium hexanoate treatment cleaved some primary  
340 esters in the Micro-Tom cutin, contrary to that observed for the cutin derived from the peels of  
341 processing tomatoes (Fig. 5D). One possibility is that the cleavage of primary esters is greatly  
342 influenced by the native arrangement of the polymer.

343 The impact of the mutations is seen by the relative abundances of aliphatics,  $\text{CH}/\text{CH}_2\text{-X}$   
344 oxygenated aliphatics, and aromatics, in the  $^1\text{H}$ -spectra which were estimated as 71%, 29% and  
345 0% for the wild-type (Fig. 6A), as 46%, 50% and 4% for *gpat6* mutant (Fig. 7A), and as 39%,  
346 59% and 2% for the *cus1* mutant (Fig. 7B), respectively. Contrary to the wild type, in both  
347 mutants the signal assigned to free acids could not be detected (Fig. 7) (Fig. 6A, *see text-inserts*).  
348 To confirm this observation, we compared the spectrum of the cutin from the *cus1* mutant  
349 purified by the ionic liquid with that of the solubilised *cus1* cuticle *via* cryogenic milling  
350 (Supplementary Fig. S16). The obtained HSQC spectra confirmed the absence of free acids in  
351 this mutant, furthering that the observed absence of this chemical group in the *cus1* and *gpat6*  
352 cutins is a consequence of the mutations and not of the sample processing.

353 Based on the  $^1\text{H}$ -spectral information, we also estimated the relative abundance of  
354 aliphatic esters (total) and primary aliphatic esters in the cutin of the mutants (Fig. 7, *see text-*  
355 *inserts*). Accordingly, the ratio of total esters *versus* linear esters is comparable in the wild type  
356 and the *gpat6* mutant but significantly lower in the *cus1* mutant. By other words, compared to the

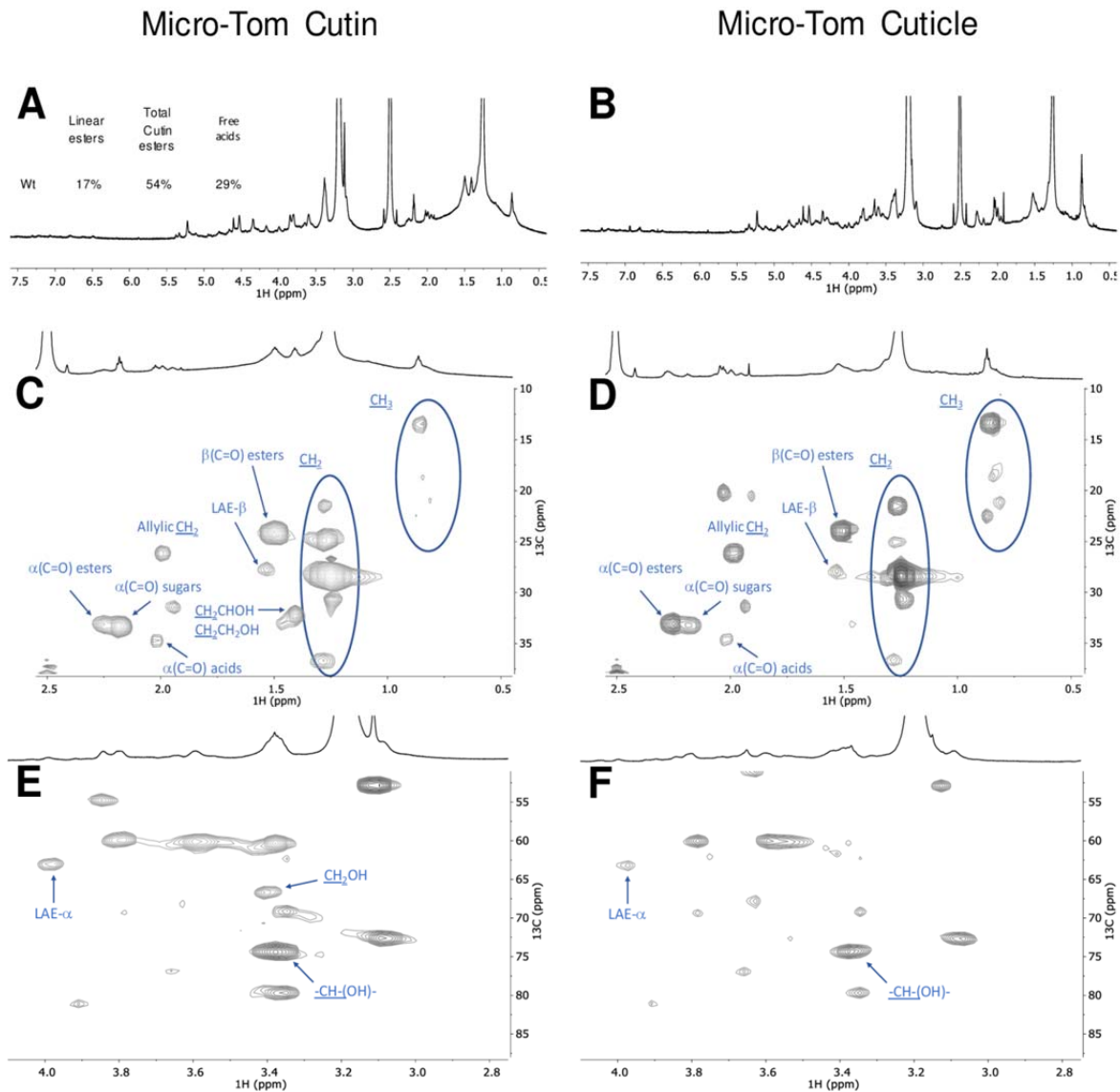


**Fig. 6.** Wide-ranging NMR spectral characterisation of Micro-tom cutin isolated with cholinium hexanoate (2 h) and Micro-tom untreated cuticle. The  $^1\text{H}$  NMR spectra of both samples (A and B, respectively), text-inserts indicate the relative abundance (%) of Linear aliphatic esters (LAE- $\alpha$ ), total esters ( $\alpha(\text{C}=\text{O})$  esters) and the free acids ( $\alpha(\text{C}=\text{O})$  acids); HSQC regions corresponding to aliphatics (C - cutin and D - cuticle) and  $\text{CH}/\text{CH}_2\text{-X}$  aliphatics (E - cutin and F - cuticle). Some correlations (unlabelled) are uncertain or unidentified.

357 wild type, the *gpat6* mutant show similar amount of linear esters and of secondary esters,

358 contrary to the *cusI* mutant that shows more than a twofold increase in linear esters but also the

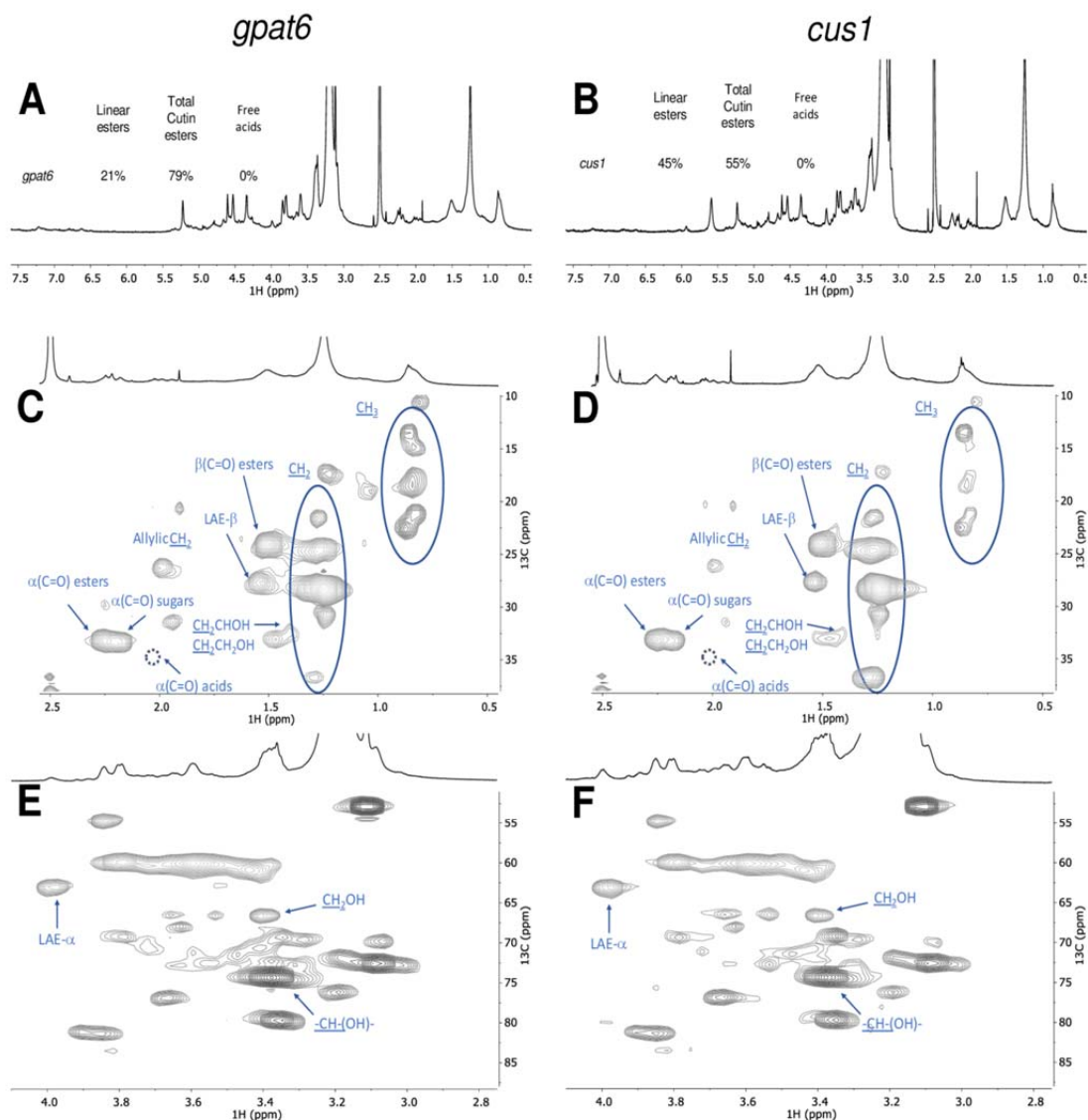


**Fig. 7.** Wide-ranging NMR spectral characterisation of Micro-Tom cutins isolated with cholinium hexanoate (2 h) from the *cus1* and *gpat6* mutants. The  $^1\text{H}$  NMR spectra of both samples (A – *cus1* and B – *gpat6*), where the text-inserts indicate the relative abundance (%) of Linear aliphatic esters (LAE- $\alpha$ ), total esters ( $\alpha(\text{C}=\text{O})$  esters) and the free acids ( $\alpha(\text{C}=\text{O})$  acids); HSQC regions corresponding to aliphatics (C – *cus1* and D – *gpat6*) and  $\text{CH}/\text{CH}_2\text{-X}$  aliphatics (E – *cus1* and F – *gpat6*). Some correlations (unlabelled) are uncertain or unidentified. The absence of the signal assigned to  $\alpha(\text{C}=\text{O})$  acids is marked by a dashed circle. For simplicity the wide-ranging NMR spectrum of the untreated cuticle from the *cus1* mutant is not shown (detailed in Supplementary Fig. S16).

359 lowest esterification level (*i.e.* amount of secondary esters) (Fig. 7A-B, *see text-insert*).

360           The magnification of the HSQC regions corresponding to aliphatics and CH/CH<sub>2</sub>-X  
361 aliphatics for the cutins of the mutants is also shown (Fig. 7C-F). For both mutants, the signals  
362 assigned to terminal hydroxyls are visible (Fig. 7E-F), similar to that observed in the wild type  
363 cutin (Fig. 6E). The detected CH<sub>3</sub> groups are apparently enriched in both mutants compared to  
364 the wild type, consistent with the observed increase in the relative abundance of hydrolysable  
365 fatty acids for the mutants (Table 3) and with that reported before (Petit et al., 2016; Philippe et  
366 al., 2016). No acylglycerol was visible in the HSQC spectra of the cutin from the mutants,  
367 possibly as their abundance are below the detection limits of the analytical technique. The  
368 mutants show more non-assigned signals compared to the wild-type cutin, consistent with the  
369 observed lower identification yields in the GC-MS (Table 3). This might reflect also an altered  
370 diversity of cuticular-polysaccharides in the mutants; one hypothesis that deserves further  
371 analysis in the near future and is sustained by the recently published results on *cus1* mutant  
372 (Philippe et al., 2020).

373

374

## 375 **Discussion**

376 Considerable advances have been made in the recent years on cuticle formation and properties  
377 (Nawrath et al., 2013). However, while the successive steps of cutin biosynthesis, transport of  
378 precursors and polymerisation in the epidermal cell walls begin to be well untangled (Fich et al.,  
379 2016), the questions of the fine structure of the cutin layer and its association with  
380 polysaccharides are still largely unresolved (Philippe et al., 2020). An example of the intricate  
381 relationships between cutin, cell walls and resistance to pathogens is that provided by the tomato  
382 *gpat6* mutant analysed herein in which the mutation has a profound impact not only on cutin  
383 synthesis (Petit et al., 2016) but also on cell walls (Philippe et al., 2020) and resistance to  
384 filamentous pathogens (Fawke et al., 2019). New insights into the structure and composition of  
385 native *gpat6* cutin would considerably help deciphering the underlying mechanisms. More  
386 generally, the simple and rapid cutin extraction method described here, which preserves cutin in  
387 a near native state, will help our understanding of the role of cuticle in plant evolution and  
388 diversity (Yeats et al., 2012; Yeats et al., 2014), plant development (Ingram and Nawrath, 2017),  
389 mechanical properties of the organ surface (España et al., 2014; Mazurek et al., 2017), resistance  
390 to pathogens (Chassot et al., 2007) and fruit quality (Petit et al., 2017).

### 391 **Advantages of ionic liquid extraction with respect to conventional cutin extraction methods**

392 Our ionic liquid cutin extraction method performed on tomato peels demonstrates that  
393 subcuticular polysaccharides (which were found in the filtrate) are removed similar to that of the  
394 enzyme treatment but in a considerable shorter period of time (*i.e.* 2 h instead of days, and even  
395 weeks) (Chatterjee et al., 2012). Also, the ionic liquid extraction does not require any specific  
396 dewaxing step. When extracted with either ionic liquid, a cutin-continuum is isolated,  
397 strengthening that the ionic liquid does not impact significantly the cutin polyester. This opposes  
398 to that previously reported by us for suberin extraction from cork using cholinium hexanoate  
399 where nanoparticles of the biopolymer are isolated (Correia et al., 2020) since the ionic liquid  
400 catalyses the mild cleavage of acylglycerol ester bonds (Ferreira et al., 2014) (which are not  
401 representative in tomato cutin).

### 402 **Cholinium hexanoate extraction preserves features of cuticular polysaccharides**

403 In the present study, the purification of the cutin-continuum by the ionic liquids is essentially due  
404 to the dissolution of the subcuticular polysaccharides and at a minor extent to ester cleavage.  
405 Under the conditions of the extraction here used, both ionic liquids cleaved very inefficiently the

406 esters bonds; however, cholinium hexanoate apparently cleaves only the acylglycerol bonds,  
407 whereas BMIM acetate can cleave also linear esters bonds. Hence, the cholinium hexanoate  
408 presents the advantage of biocompatibility and of a milder cleavage of the polymer backbone.  
409 Their most remarkable difference is that only the cholinium hexanoate could preserve features of  
410 cuticular polysaccharides, which were specifically associated to the presence of microcrystalline  
411 cellulose. Cellulose with high levels of crystallinity was recently identified within the group of  
412 cutin embedded polysaccharides (Philippe et al., 2020), consistent with the ability of the used  
413 ionic liquid process for a speedy recovery of cutin with a near native structure. This opens  
414 unexpected possibilities for exploiting both ionic liquids, alone or in combination, to study the  
415 association and function of cuticular polysaccharides.

#### 416 **Cholinium hexanoate extraction confirms the presence of free hydroxyls in native cutin and** 417 **highlights differences in free fatty acid composition between wild type and mutants**

418 Finally, the solution NMR spectra of cutins purified by cholinium hexanoate and of the matching  
419 cuticles (both of which solubilised with the aid of cryogenic milling) strengthened that some free  
420 hydroxyls exist *in situ*, consistent with that previously reported by others (Petit et al., 2016;  
421 Philippe et al., 2016). Results from a systematic NMR analysis of cutins purified by cholinium  
422 hexanoate from both wild-type and mutants of the same genotype (Micro-Tom) show increased  
423 diversity of fatty acids in both mutants yet only the *cus1* mutant show a significantly reduced  
424 esterification degree. These results are consistent with the function of the enzymes  
425 inactivated: *cus1* is a polymerizing enzyme (Girard et al., 2012; Yeats et al., 2012)  
426 while *gpat6* catalyses the synthesis of cutin precursors (Petit et al., 2016). Remarkably, these  
427 results are also consistent with already published information on the mutants, which were  
428 obtained through a totally independent approach (Philippe et al., 2016). *In situ* analysis of cutin  
429 esterification levels by benzyl etherification of enzyme-treated cutin from tomato fruit peel  
430 showed that all/midchain hydroxylation of dihydroxy acids is increased strongly in *cus1* (linear  
431 polymers) but remained unaffected in *gpat6* mutant, as in wild type (normal inter-branching).

432 Remarkably, the NMR results of the ionic liquid extracted cutins are strongly suggestive  
433 that naturally occurring free acids exists in the wild-type tomatoes (detected also in the cuticle)  
434 however lacking in the mutants (lacking also in their cuticles, as observed for the *cus1* cuticle).  
435 This might be due to the thinner mutant cuticles where a total esterification of the cutin  
436 monomers could be more easily achieved. This deserves a detailed analysis in the near future,

437 especially as: (i) we could not yet detect the signal assigned to  $\beta(\text{C}=\text{O})$  acid, only that of the  
438  $\alpha(\text{C}=\text{O})$  acids that was assigned through HMBC spectrum, and (ii) the signal assigned to the  
439  $\alpha(\text{C}=\text{O})$  esters partially overlaps with that of the  $\alpha(\text{C}=\text{O})$  sugars in the analysed tomato cutins.

440

## 441 **Conclusions**

442 The proof-of-concept of the efficiency and reliability of the ionic liquid cutin extraction method  
443 described here was done using tomato peel as a model. Because of its simplicity, this method  
444 should be broadly applicable to other tissues and to other plant model and crop species, as  
445 confirmed by preliminary experiments. In the near future quantitative methods (and better  
446 spectral resolution for solving yet unknown signals) will require development in order to  
447 understand better how cutin molecular structure (and its association with cuticular  
448 polysaccharides) is impacted by mutations or along the development of the plant. In addition, our  
449 study emphasises the suitability of exploiting ionic liquid extractions as an easy and scalable  
450 approach for exploiting plant lipid polymers as a bio-resource for a diversity of applications. The  
451 ionic liquid processes here tested can be systematically tuned, *e.g.* time, temperature, composing  
452 ions, to ensure recovery of a cutin with different degrees of structural preservation. Finally, the  
453 solution NMR methodologies developed here constitute now essential tools to fingerprint the  
454 multi-functionality and the structure of cutin *in planta*. Based on all the analyses done on the  
455 polymer morphology, thermal properties and chemistry, we are confident that short-time  
456 reactions with cholinium hexanoate can ensure the isolation of cutin carrying minimal disruption  
457 of its polymeric network – yielding the closest to a native configuration reported to date.

458

## 459 **Material and Methods**

### 460 **Plant Material**

461 Peels from the processing tomato (*Solanum lycopersicum* ‘Roma’) were manually removed,  
462 thoroughly washed and then dried until constant weight at 60 °C. After drying, the peels were  
463 milled using a Retsch ZM200 electric grinder (granulometry 0.5 mm; 10000 rpm) and stored at  
464 room temperature for further processing. Micro-Tom cultivar tomatoes from both wild type and  
465 mutants plants (which were generated by an ethyl methanesulfonate (EMS) mutagenesis (Just et



466 al., 2013)) were cultivated as previously reported (Rothan et al., 2016), and processed as  
467 described above. All tomato fruits used were in the red ripe developmental stage.

#### 468 **Chemicals**

469 1-butyl-3-methyl-imidazolium acetate (>98%) was purchased from io-li-tec; sodium hydroxide  
470 (>98%) from José Manuel Gomes dos Santos; methanol ( $\geq 99.8\%$ ), dimethyl sulfoxide (DMSO,  
471 >99.99%), hexane (>95%), chloroform (>99.98%), dichloromethane (>99.99%) from Fisher  
472 Chemical; cholinium hydrogen carbonate (~80% in water), hexanoic acid (>99.5%), sodium  
473 azide ( $\geq 99.5\%$ ), sodium acetate ( $\geq 99\%$ ), cellulase (*Aspergillus niger*) and pectinase (*Aspergillus*  
474 *aculeatus*) from Sigma Aldrich. Cholinium hexanoate was synthesised by dropwise addition of  
475 hexanoic acid to aqueous cholinium hydrogen carbonate in equimolar quantities, as previously  
476 described (Petkovic et al., 2010).

#### 477 **Ionic liquid hydrolysis of standard fatty acids**

478 Glycerol trioctanoate and octyl octanoate (*ca.* 50 mg) were mixed with either ionic liquid (1:10  
479 ratio) at 100 °C, without stirring, during 2, 6 or 24 hours. At the end of the reaction, the mixture  
480 was rapidly cooled to room temperature in ice, acidified to pH 3/3.5 with 1 M HCl solution,  
481 spiked with a known concentration of heptadecanoic acid (internal standard), and extracted three  
482 times using dichloromethane/water partition. The dried combined organic phases were  
483 derivatised with N,O-bis(trimethylsilyl)trifluoroacetamide in pyridine (5:1), during 30 min at 90  
484 °C. The TMS derivatives in the organic fractions were then analysed by GC-MS as previously  
485 described (Ferreira et al., 2014) with minor modifications (ramp temperature: 60 °C, 4 °C/min  
486 until 280 °C during 15 min, with source at 230 °C and electron impact ionization of 70 eV) (see  
487 equipment below). Triplicate independent reactions were performed.

#### 488 **Cutin Extractions**

489 *Enzymatic Process.* Cutin was isolated from tomato as previously described (Chatterjee et al.,  
490 2012). In brief, tomato peels were immersed in an enzymatic cocktail containing 4 ml of  
491 pectinase, 0.2 g of cellulase, 13 mg NaN<sub>3</sub> and 196 ml of 50 mM sodium acetate buffer, and  
492 incubated at 31 °C for 24 hours with constant shaking. The isolated cuticles were successively  
493 dewaxed during 36 hours by Soxhlet extraction with methanol, chloroform and hexane (1:1:1),  
494 finally freeze dried and stored at room temperature. This cutin is used as a reference material in  
495 the present study.

496 *Ionic liquid Process.* Cutin was extracted from tomato peels as previously described for the  
497 extraction of suberin from cork (Ferreira et al., 2014), with slight modifications. In brief, 2 g of  
498 tomato peel powder were mixed in 20 g cholinium hexanoate or BMIM acetate and incubated for  
499 a defined period of time (100 °C, without stirring). The reaction was stopped by the addition of  
500 160 mL of DMSO. The polymer was recovered by filtration using a nylon membrane filter (0,45  
501 µm); then washed with an excess of deionized water with the aid of centrifugation (Eppendorf  
502 5804 R centrifuge, 5000 rpm at 4 °C for 30 minutes).

### 503 **Treatment of cutin extracted using cholinium hexanoate (2h) with Trifluoroacetic Acid**

504 600 mg of the cutin obtained through extraction with cholinium hexanoate for 2 h were treated  
505 with 1 M of aqueous TFA solution during 60 minutes at 110 °C. The reaction mixture was  
506 filtered, and the insoluble material was washed with stirring using chloroform-methanol (1:1 v/v)  
507 for 2 h. The organic-insoluble material was separated by filtration, freeze-dried, and analysed by  
508 <sup>13</sup>C MAS NMR.

509 **Microscopic analyses.** Scanning electron microscopy (SEM) (microscope JEOL JSM-7001F)  
510 was used to analyse the cutin samples.

### 511 **Cryogenic grinding process**

512 A RESTCH Cryomill equipped with a 25 mL grinding jar with 6 zirconium oxide grinding balls  
513 (10 mm) was used. To optimise the solubilisation level of cutin needed for attaining high NMR  
514 spectral resolution, cutin samples were cryogenically milled at -196 °C (liquid nitrogen) as  
515 follows: 3 min of pre-cooling followed by 9 milling cycles, each comprising 3 min of milling at  
516 30 Hz plus 0.5 min of intermediate cooling at 5 Hz. The ensuing samples were analysed by <sup>1</sup>H  
517 NMR (3 mg dissolved in 400 µL of DMSO-*d*<sub>6</sub>) and the 200 milling cycles were selected for  
518 systematically process cutin samples prior to their 2D NMR analysis.

### 519 **Nuclear Magnetic Resonance (NMR) analyses.**

520 Solution state NMR spectra were recorded using an Avance II + 800 MHz (Bruker Biospin,  
521 Rheinstetten, Germany) spectrometers, with exception of <sup>1</sup>H-<sup>13</sup>C HMBC spectra that were  
522 acquired using an Avance III 800 CRYO (Bruker Biospin, Rheinstetten, Germany). All NMR  
523 spectra (<sup>1</sup>H, <sup>1</sup>H-<sup>1</sup>H COSY, <sup>1</sup>H-<sup>13</sup>C HSQC) were acquired in DMSO-*d*<sub>6</sub> using 5 mm diameter  
524 NMR tubes, at 60 °C as follows: 3 mg of cryomilled cutin in 400 µL of DMSO-*d*<sub>6</sub>. <sup>13</sup>C Magic  
525 Angle Spinning Nuclear Magnetic Resonance (<sup>13</sup>C MAS NMR) spectra were acquired on cutin  
526 samples (± 250 mg) were packed into 7 mm o.d. zirconia rotors (after grinded if needed),

527 equipped with Kel-F caps.  $^{13}\text{C}$  MAS with High-Power CW Decoupling spectra were obtained at  
528 75.49 MHz, on a Tecmag Redstone/Bruker 300WB, with spinning rates of 3.1-3.3 kHz. In these  
529 experiences  $90^\circ$  RF pulses of around 4.5  $\mu\text{s}$  and relaxation delays of 3 s were used.  $^{13}\text{C}$  chemical  
530 shifts were referenced with respect to external glycine ( $^{13}\text{CO}$  observed at 176.03 ppm).  
531 MestReNova, Version 11.04-18998 (Mestrelab Research, S.L.) was used to process the raw data  
532 acquired in the Bruker spectrometers.

### 533 **Differential scanning calorimetry (DSC)**

534 Calorimetric analyses were carried out in a TA Instruments Q200 calorimeter connected to a  
535 cooling system and calibrated with different standards (indium, empty cap). The sample weights  
536 ranged from 9 to 11 mg. A temperature interval from  $-80^\circ\text{C}$  to  $220^\circ\text{C}$  has been studied and the  
537 used heating/cooling rate was  $10^\circ\text{C}\cdot\text{min}^{-1}$ .

### 538 **Wide-Angle X-ray Scattering (WAXS)**

539 WAXS data were collected using a laboratory SAXS/WAXS beamline (Xeuss 2.0, Xenocs,  
540 Grenoble, France) equipped with a liquid gallium MetalJet X-ray source (Excillum, Sweden)  
541 (wavelength  $\lambda = 1.34 \text{ \AA}$ ), FOX 3D Ga single reflection X-ray mirror and two two sets of  
542 motorized scatterless slits for beam collimation, and a Pilatus 100k two-dimensional (2D) pixel  
543 WAXS detector (Dectris, Switzerland). Loose cutin powder samples were enclosed between two  
544 flat kapton films and mounted on the beamline sample stage (the total sample thickness is about  
545 1 mm). 2D WAXS patterns were recorded in a transmission mode over a  $q$  range of  $1.3 \text{ \AA}^{-1}$  to  $3.5$   
546  $\text{ \AA}^{-1}$  [where  $q = (4\pi\sin\theta)/\lambda = 2\pi/d$  is the length of the scattering vector,  $\theta$  is one-half of the  
547 scattering angle and  $d$  is spacing in real space] using exposure time of 1200 seconds. The WAXS  
548 data were reduced (calibrated, integrated and background-subtracted) using the Foxtrot software  
549 package supplied with the instrument.

### 550 **Gas Chromatography-Mass Spectrometry (GC-MS)**

551 An Agilent gas chromatograph (7820A) equipped with an Agilent (5977B) mass spectrometer  
552 (quadrupole) was used. First, to release the hydrolysable constituents, the samples were treated  
553 with a solution of 0.5 M NaOH in methanol/water (1:1, v/v) at  $95^\circ\text{C}$ , during 4 hours; cooled to  
554 room temperature and acidified to pH 3/3.5 with 1 M HCl, then extracted by  
555 dichloromethane/water partition (5X). The non-hydrolysable fraction was recovered by filtration  
556 ( $0.2 \mu\text{m}$ , nylon filters), washed, freeze-dried, and weighted (recalcitrance). The dried combined  
557 organic extracts were sequentially derivatised (30 min,  $90^\circ\text{C}$ ): firstly, 2.0 M

558 (trimethylsilyl)diazomethane in hexane, mixed in a methanol:toluene 2.5:1 solution (3:2); and  
559 secondly, N,O-bis(trimethylsilyl)trifluoroacetamide containing 1% of trimethylchlorosilane in  
560 pyridine (5:1). The derivatives were then analysed by GC-MS (HP-5MS column) with the  
561 following ramp temperature: 80 °C, 4 °C/min until 310 °C during 15 min. MS scan mode, with  
562 source at 230 °C and electron impact ionization (EI+, 70 eV) was used for all samples. The GC-  
563 MS was first calibrated with pure reference compounds (representative monomers:  
564 heptadecanoic acid, hexadecanedioic acid and ferulic acid) relative to hexadecane (internal  
565 standard). Each sample was analysed in triplicates. Data acquisition was accomplished by MSD  
566 ChemStation (Agilent Technologies); compounds were identified based on the equipment  
567 spectral library (Wiley-NIST) and references relying on diagnostic ions distinctive of each  
568 derivative and its spectrum profile (Supplementary Table S1).

569

## 570 **Acknowledgments**

571 We acknowledge funding from the European Research Council through grant ERC 2014-CoG-  
572 647928, from the European Union's Horizon 2020 research and innovation programme within  
573 the project 713475 – FLIPT – H2020-FETOPEN-2014-2015 and from Fundação para a Ciência e  
574 Tecnologia (FCT) through the grant UID/Multi/04551/2019 (Research unit GREEN-it  
575 "Bioresources 4 Sustainability") and the projects PTDC/AGR-TEC/1191/2014AAC. The  
576 solution NMR data was acquired at CERMAX, ITQB-NOVA, Oeiras, Portugal with equipment  
577 funded by FCT. C.J.S.M. is grateful to Aralab, Portugal, for the PhD contract  
578 06/PlantsLife/2017. O.O.M. thanks EPSRC for a capital equipment grant to purchase the  
579 Xenocs/Excillum SAXS/WAXS laboratory beamline (EP/M028437/1). The authors are thankful  
580 to Manolis Matzapetakis (ITQB NOVA) and to Maria João Ferreira (IST) for support in the  
581 solid-state NMR analyses, and to Pedro Lamosa and Maria C. Leitão (ITQB NOVA) for support  
582 in the solution NMR and chromatographic analyses, respectively. Finally, we are extremely  
583 grateful to Bénédicte Bakan and Didier Marion for fruitful scientific discussions during the  
584 manuscript preparation.

585

## 586 Captions Tables and Figures

587

588 **Table 1.** Relative abundance of the contributions of the region of the aliphatics (10-50 ppm),  
589 oxygenated aliphatics (57-92 ppm), aromatics (92-165 ppm) and carboxyl groups (165-185 ppm)  
590 for each cutin  $^{13}\text{C}$  MAS NMR spectrum.

591

592 **Table 2.** GC-MS quantitative analysis of the hydrolysable constituents identified in cutin  
593 samples purified using either cholinium hexanoate or 1-butyl-3-methylimidazolium acetate (2,  
594 15 or 170 h reactions). The reference cutin and the feedstock (*i.e.* untreated peels) were also  
595 analysed for comparison. Results are given as % (wt) ( $n=3$ ). The identification yields (wt %) and  
596 the mass of the non-hydrolysable fraction (recalcitrance, %) are indicated below.

597

598 **Table 3.** GC-MS quantitative analysis of the hydrolysable constituents in cutin samples purified  
599 using cholinium hexanoate (2 h reaction) from Micro-Tom tomatoes: wild type, *cus1* and *gpat6*  
600 plants. Results are given as % (wt) ( $n=3$ ). The identification yields (wt %) and the mass of the  
601 non-hydrolysable fraction (recalcitrance, %) are indicated below.

602

603 **Fig. 1.** Compounds detected after the reaction of glyceryl trioctanoate and octyl octanoate with  
604 either cholinium hexanoate (A) or 1-butyl-3-methylimidazolium acetate (B) for 2, 6 and 24 hours  
605 (the observed average standard errors were negligible, < 4%). All compounds were identified  
606 and quantified by GC-MS. At time zero, glyceryl trioctanoate and octyl octanoate were assumed  
607 to represent the only compounds present in mixture.

608

609 **Fig. 2.** SEM imaging of cutin purified after treatment with cholinium hexanoate (B-D) or 1-  
610 butyl-3-methylimidazolium acetate (E-G) after 2, 15 and 170 hours. All samples show a clean  
611 thick cutin-continuum comprising the epidermal cells grooves. A representative cutin reference  
612 sample (*i.e.* obtained through the conventional enzymatic-based process) is also shown denoting  
613 many intracellular spaces that are not hollow (A).

614

615 **Fig. 3.**  $^{13}\text{C}$  MAS NMR spectra obtained for the cutin reference and the cutin samples derived  
616 from reactions with cholinium hexanoate or 1-butyl-3-methylimidazolium acetate after 2, 15 and

617 170 hours (A) and the corresponding calculated reticulation (B-C) and esterification (D) ratios.  
618 The regions assigned to the long methylene chains, the oxygenated aliphatics, aromatics and the  
619 carboxyl groups are marked. The imidazolium-based cation contributes to the signal assigned to  
620 the CH<sub>3</sub> groups (15 ppm<sup>\*\*</sup>), whereas the cholinium cation is seen in the signal at 54 ppm<sup>\*</sup>; both  
621 contaminants can be washed out.

622  
623 **Fig. 4.** DSC thermograms (A) and WAXS patterns (B) collected for a reference enzymatically-  
624 extracted cutin (black curve) and cutin powders extracted from tomato peels using ionic liquids  
625 for various durations of the treatment [cholinium hexanoate (purple curve for 2 hours and blue  
626 curve for 170 hours) and imidazolium acetate (cyan curve for 2 hours and grey curve for 170  
627 hours)]. The vertical straight lines in WAXS patterns indicate position of diffraction peaks of  
628 cellulose (dotted lines) and crystallised *n*-alkane chains (dashed lines). Miller indexes assigned to  
629 the lines correspond to cellulose I<sub>β</sub> (monoclinic space group P12<sub>1</sub>1) and *n*-alkane chain packing  
630 (orthorhombic space group Pnma).

631  
632 **Fig. 5.** Wide-ranging NMR spectral characterisation of cutin isolated with cholinium hexanoate  
633 (2 h). The <sup>1</sup>H NMR, with inserts focussing the aliphatic and oxygenated aliphatics regions (A);  
634 and the HSQC spectrum: full (B) and regions corresponding to aliphatics (C) and CH/CH<sub>2</sub>-X  
635 aliphatics (D) of the purified cutin. Some correlations (unlabelled) are uncertain or unidentified.

636  
637 **Fig. 6.** Wide-ranging NMR spectral characterisation of Micro-Tom cutin isolated with cholinium  
638 hexanoate (2 h) and Micro-Tom untreated cuticle. The <sup>1</sup>H NMR spectra of both samples (A –  
639 cutin and B - cuticle), where the text-inserts indicate the relative abundance (%) of Linear  
640 aliphatic esters (LAE-α), total esters (α(C=O) esters) and the free acids (α(C=O) acids); HSQC  
641 regions corresponding to aliphatics (C - cutin and D - cuticle) and CH/CH<sub>2</sub>-X aliphatics (E -  
642 cutin and F - cuticle). Some correlations (unlabelled) are uncertain or unidentified.

643  
644 **Fig. 7.** Wide-ranging NMR spectral characterisation of Micro-Tom cutins isolated with  
645 cholinium hexanoate (2 h) from the *cus1* and *gpat6* mutants. The <sup>1</sup>H NMR spectra of both  
646 samples (A – *cus1* and B – *gpat6*), where the text-inserts indicate the relative abundance (%) of  
647 Linear aliphatic esters (LAE-α), total esters (α(C=O) esters) and the free acids (α(C=O) acids);

648 HSQC regions corresponding to aliphatics (C – *cus1* and D – *gpat6*) and CH/CH<sub>2</sub>-X aliphatics (E  
649 – *cus1* and F - *gpat6*). Some correlations (unlabelled) are uncertain or unidentified. The absence  
650 of the signal assigned to  $\alpha(\text{C}=\text{O})$  acids is marked by a dashed circle. For simplicity the wide-  
651 ranging NMR spectrum of the untreated cuticle from the *cus1* mutant is not shown (detailed in  
652 Supplementary Fig. S16).  
653

654 **Table 1**

655

		<b>Relative abundance of the <sup>13</sup>C MAS NMR assigned regions (%)</b>				
<b>Method</b>	Cutin major structural classes	<b>C=O</b>	<b>C=C</b>	<b>CHO</b>	<b>CH<sub>2</sub>O</b>	<b>(CH<sub>2</sub>)<sub>n</sub></b>
		carboxyl	aromatics	oxygenated	aliphatics	aliphatics
Reference	-	5.1	1.7	5.1	2.6	85.5
Cholinium hexanoate	2 h	4.8	1.6	9.6	3.7	80.0
	2 h + TFA	3.9	3.1	10.2	4.7	78.1
	15 h	4.7	3.1	10.9	3.9	77.5
	170 h	4.7	3.1	9.1	3.9	65.0
Imidazolium acetate	2 h	5.6	4.0	7.2	3.2	80.0
	15 h	5.5	5.5	7.8	3.1	73.5
	170 h	5.6	6.5	4.0	3.2	80.6

656

657

658



**Table 2**

Compound name	Compound abundance % (wt)							
	Untreated feedstock	Reference cutin	cholinium hexanoate			BMIM acetate		
			2h	15h	170h	2h	15h	170h
<b>FATTY ACIDS</b>	<b>2.60 ± 0.13</b>	<b>1.52 ± 0.24</b>	<b>1.27 ± 0.15</b>	<b>0.88 ± 0.13</b>	<b>0.67 ± 0.09</b>	<b>1.96 ± 0.2</b>	<b>0.74 ± 0.1</b>	<b>0.10 ± 0.06</b>
hexadecanoic acid	1.25 ± 0.04	0.74 ± 0.05	0.64 ± 0.04	0.41 ± 0.11	0.33 ± 0.03	0.63 ± 0.05	0.42 ± 0.03	0.10 ± 0.06
octadeca-9,12-dienoic acid	0.43 ± 0.15	0.23 ± 0.05	0.20 ± 0.03	0.11 ± 0.01		0.74 ± 0.12		
octadec-9-enoic acid		0.24 ± 0.06	0.11 ± 0.02	0.09 ± 0.04		0.18 ± 0.03		
octadecanoic acid	0.91 ± 0.12	0.31 ± 0.10	0.09 ± 0.00	0.13 ± 0.05	0.12 ± 0.02	0.18 ± 0.04	0.13 ± 0.06	
4-oxocyclohexane-1-carboxylic acid			0.23 ± 0.08	0.14 ± 0.12	0.22 ± 0.06	0.23 ± 0.00	0.19 ± 0.02	
<b>DICARBOXYLIC ACIDS</b>	<b>10.89 ± 1.08</b>	<b>18.38 ± 0.44</b>	<b>18.64 ± 0.49</b>	<b>19.2 ± 2.16</b>	<b>18.64 ± 0.58</b>	<b>18.45 ± 1.19</b>	<b>19.3 ± 0.21</b>	<b>9.99 ± 2.05</b>
nonanedioic acid <sup>(a)</sup>		0.43 ± 0.02	0.26 ± 0.02	0.26 ± 0.15	0.36 ± 0.01	0.27 ± 0.02	0.22 ± 0.04	
hexadecanedioic acid	0.56 ± 0.02	1.51 ± 0.07	1.30 ± 0.07	1.52 ± 0.10	1.22 ± 0.08	1.47 ± 0.07	1.42 ± 0.15	0.46 ± 0.07
8/9-hydroxyhexadecanedioic acid <sup>(b)</sup>	10.33 ± 1.06	16.43 ± 0.38	17.08 ± 0.55	17.43 ± 2.01	17.06 ± 0.50	16.7 ± 1.14	17.66 ± 0.20	9.53 ± 0.23
<b>ω-HYDROXY ACIDS</b>	<b>11.13 ± 0.35</b>	<b>15.04 ± 0.31</b>	<b>18.42 ± 0.63</b>	<b>17.42 ± 2.22</b>	<b>17.69 ± 1.28</b>	<b>18.95 ± 0.4</b>	<b>18.49 ± 1.06</b>	<b>22.90 ± 1.68</b>
16-hydroxyhexadecanoic acid	5.38 ± 0.16	8.17 ± 0.21	8.20 ± 0.12	8.50 ± 0.65	8.32 ± 0.21	8.35 ± 0.23	8.48 ± 0.39	15.71 ± 0.66
16-hydroxy-10-oxohexadecanoic acid	3.02 ± 0.28	2.29 ± 0.14	6.39 ± 0.52	6.21 ± 0.97	6.28 ± 0.61	6.81 ± 0.05	6.62 ± 0.39	1.80 ± 0.12
9, 10-epoxy-18-hydroxyoctadecanoic acid	1.14 ± 0.24	1.93 ± 0.09	1.73 ± 0.07	1.63 ± 0.38	1.27 ± 0.32	1.67 ± 0.13	1.60 ± 0.14	2.38 ± 0.53
9, 10-epoxy-18-hydroxyoctadecenoic acid	1.60 ± 0.15	2.65 ± 0.20	2.10 ± 0.25	1.62 ± 0.18	1.82 ± 0.55	2.11 ± 0.09	1.79 ± 0.18	3.01 ± 0.59
<b>POLYHYDROXYACIDS</b>	<b>55.05 ± 2.01</b>	<b>65.06 ± 0.65</b>	<b>61.67 ± 0.28</b>	<b>62.49 ± 4.06</b>	<b>63.01 ± 1.92</b>	<b>60.64 ± 1.69</b>	<b>61.47 ± 1.28</b>	<b>67.01 ± 1.44</b>
10,16-dihydroxyhexadecanoic acid <sup>(c)</sup>	53.22 ± 2.23	63.24 ± 0.98	58.83 ± 0.42	59.68 ± 5.03	61.20 ± 2.16	58.12 ± 1.89	58.97 ± 1.55	63.12 ± 2.42
9,10,18-trihydroxyoctadecanoic acid	1.00 ± 0.11	0.94 ± 0.06	1.11 ± 0.32	1.19 ± 0.67	0.53 ± 0.00	0.85 ± 0.11	0.90 ± 0.13	1.51 ± 0.45
9,10,18-trihydroxyoctadec-12-enoic acid	0.84 ± 0.39	0.89 ± 0.36	1.73 ± 0.07	1.63 ± 0.38	1.27 ± 0.32	1.67 ± 0.13	1.60 ± 0.14	2.38 ± 0.53
<b>STEROLS*</b>	<b>20.33 ± 1.07</b>							
<b>Identification Yield (%)</b>	<b>56.38 ± 2.46</b>	<b>50.7 ± 2.38</b>	<b>58.1 ± 0.88</b>	<b>59.34 ± 6.63</b>	<b>56.39 ± 1.20</b>	<b>58.02 ± 2.45</b>	<b>60.35 ± 3.46</b>	<b>82.15 ± 0.20</b>
<b>Recalcitrance (%)</b>	<b>22.14 ± 2.98</b>	<b>13.32 ± 1.39</b>	<b>28.3 ± 4.98</b>	<b>27.47 ± 0.58</b>	<b>33.07 ± 0.56</b>	<b>19.75 ± 0.36</b>	<b>20.21 ± 1.06</b>	<b>18.15 ± 2.48</b>

(a) Overestimated, overlapped with an unknown compound; (b) With possible presence of unspecific isomers; (c) Major 10,16-diOH, minors 9,16 and 8,16-*di*-OH.

\*Identified triterpenoids and sterols: β-amyrin (5.69 ± 0.44); α-amyrin (4.44 ± 0.20); δ-amyrin (7.53 ± 1.48) and stigmasterol (2.68 ± 0.49).

660

**Table 3**

Compound name	Compound abundance % (wt)		
	cholinium hexanoate (2 h)		
	<i>wt</i>	<i>cus1</i>	<i>gpat6</i>
<b>FATTY ACIDS</b>	<b>0.50 ± 0.04</b>	<b>6.06 ± 0.81</b>	<b>5.60 ± 0.88</b>
hexadecanoic acid	0.27 ± 0.02	2.09 ± 0.26	1.59 ± 0.23
9,12-octadecadienoic		3.00 ± 0.59	2.22 ± 0.42
9-octadecenoic acid	0.24 ± 0.06		1.20 ± 0.16
octadecanoic acid		0.96 ± 0.12	0.59 ± 0.11
<b>DICARBOXYLIC ACIDS</b>	<b>4.68 ± 0.32</b>	<b>7.23 ± 0.55</b>	<b>7.92 ± 0.5</b>
nonanedioic acid <sup>(a)</sup>		1.75 ± 0.37	0.88 ± 0.05
hexadecandioic acid	0.60 ± 0.10		1.95 ± 0.23
8/9-hydroxyhexadecanedioic acid <sup>(b)</sup>	4.08 ± 0.23	5.48 ± 0.24	5.09 ± 0.25
<b>ω-HYDROXY ACIDS</b>	<b>5.47 ± 0.30</b>	<b>1.19 ± 0.02</b>	<b>1.56 ± 0.08</b>
16-hydroxyhexadecanoic acid	3.97 ± 0.23	1.19 ± 0.02	1.12 ± 0.09
16-hydroxy-10-oxohexadecanoic acid	0.71 ± 0.04		0.44 ± 0.02
9, 10-epoxy-18-hydroxyoctadecanoic acid	0.25 ± 0.05		
9, 10-epoxy-18-hydroxyoctadecenoic acid	0.54 ± 0.02		
<b>POLYHYDROXYACIDS</b>	<b>89.35 ± 0.63</b>	<b>85.33 ± 1.32</b>	<b>84.86 ± 1.46</b>
dihydroxyhexadecanoic acid <sup>(c)</sup>	87.91 ± 0.48	83.87 ± 1.52	77.71 ± 2.50
9,10,18-trihydroxyoctadecanoic acid	0.62 ± 0.06	0.91 ± 0.18	3.84 ± 0.76
9,10,18-trihydroxyoctadec-12-enoic acid	0.82 ± 0.09	0.54 ± 0.04	3.31 ± 0.49
<b>STEROLS*</b>		<b>0.19 ± 0.04</b>	
<b>Identification Yield (%)</b>	57.99 ± 1.26	37.49 ± 0.74	36.05 ± 1.75
<b>Recalcitrance (%)</b>	32.6 ± 3.68	44.26 ± 2.96	41.28 ± 0.97

(a) Overestimated, overlapped with an unknown compound; (b) With possible presence of unspecific isomers; (c) Major 10,16-diOH, minors 9,16 and 8,16-*di*-OH.

\*Identified sterols: stigmasterol

661

662



## Parsed Citations

**Arrieta-Baez D, Stark RE (2006) Using Trifluoroacetic Acid To Augment Studies of Potato Suberin Molecular Structure. J Agric Food Chem 54: 9636–9641**

Pubmed: [Author and Title](#)

Google Scholar: [Author Only Title Only Author and Title](#)

**Bakan B, Marion D (2017) Assembly of the Cutin Polyester: From Cells to Extracellular Cell Walls. Plants 6: 57**

Pubmed: [Author and Title](#)

Google Scholar: [Author Only Title Only Author and Title](#)

**Benítez JJ, Castillo PM, del Río JC, León-Camacho M, Domínguez E, Heredia A, Guzmán-Puyol S, Athanassiou A, Heredia-Guerrero JA (2018) Valorization of tomato processing by-products: Fatty acid extraction and production of bio-based materials. Materials (Basel) 11: 2211**

Pubmed: [Author and Title](#)

Google Scholar: [Author Only Title Only Author and Title](#)

**Bunn CW (1944) The crystal structure of ethylene. Trans Faraday Soc 40: 23–25**

Pubmed: [Author and Title](#)

Google Scholar: [Author Only Title Only Author and Title](#)

**Chassot C, Nawrath C, Métraux JP (2007) Cuticular defects lead to full immunity to a major plant pathogen. Plant J 49: 972–980**

Pubmed: [Author and Title](#)

Google Scholar: [Author Only Title Only Author and Title](#)

**Chatterjee S, Matas AJ, Isaacson T, Kehlet C, Rose JKC, Stark RE (2016) Solid-state<sup>13</sup>C NMR delineates the architectural design of biopolymers in native and genetically altered tomato fruit cuticles. Biomacromolecules 17: 215–224**

Pubmed: [Author and Title](#)

Google Scholar: [Author Only Title Only Author and Title](#)

**Chatterjee S, Sarkar S, Oktawiec J, Mao Z, Niitsoo O, Stark RE (2012) Isolation and Biophysical Study of Fruit Cuticles. J Vis Exp e3529**

Pubmed: [Author and Title](#)

Google Scholar: [Author Only Title Only Author and Title](#)

**Correia VG, Bento A, Pais J, Rodrigues R, Haliński ŁP, Frydrych M, Greenhalgh A, Stepnowski P, Vollrath F, King AWT, et al (2020) The Molecular Structure and Multi-functionality of the Cryptic Plant Polymer Suberin. Mater Today Bio (in press)**

Pubmed: [Author and Title](#)

Google Scholar: [Author Only Title Only Author and Title](#)

**Deshmukh AP, Simpson AJ, Hatcher PG (2003) Evidence for cross-linking in tomato cutin using HR-MAS NMR spectroscopy. Phytochemistry 64: 1163–1170**

Pubmed: [Author and Title](#)

Google Scholar: [Author Only Title Only Author and Title](#)

**España L, Heredia-Guerrero JA, Segado P, Benítez JJ, Heredia A, Domínguez E (2014) Biomechanical properties of the tomato (*Solanum lycopersicum*) fruit cuticle during development are modulated by changes in the relative amounts of its components. New Phytol 202: 790–802**

Pubmed: [Author and Title](#)

Google Scholar: [Author Only Title Only Author and Title](#)

**Fawke S, Torode TA, Gogleva A, Fich EA, Sørensen I, Yunusov T, Rose JKC, Schornack S (2019) Glycerol-3-phosphate acyltransferase 6 controls filamentous pathogen interactions and cell wall properties of the tomato and *Nicotiana benthamiana* leaf epidermis. New Phytol 223: 1547–1559**

Pubmed: [Author and Title](#)

Google Scholar: [Author Only Title Only Author and Title](#)

**Fernández V, Guzmán-Delgado P, Graça J, Santos S, Gil L (2016) Cuticle Structure in Relation to Chemical Composition: Re-assessing the Prevailing Model. Front Plant Sci 7: 1–14**

Pubmed: [Author and Title](#)

Google Scholar: [Author Only Title Only Author and Title](#)

**Ferreira R, Garcia H, Sousa AF, Guerreiro M, Duarte FJS, Freire CSR, Calhorda MJ, Silvestre AJD, Kunz W, Rebelo LPN, et al (2014) Unveiling the dual role of the cholinium hexanoate ionic liquid as solvent and catalyst in suberin depolymerisation. RSC Adv 4: 2993–3002**

Pubmed: [Author and Title](#)

Google Scholar: [Author Only Title Only Author and Title](#)

**Ferreira R, Garcia H, Sousa AF, Petkovic M, Lamosa P, Freire CSR, Silvestre AJD, Rebelo LPN, Silva Pereira C (2012) Suberin isolation from cork using ionic liquids: Characterisation of ensuing products. New J Chem 36: 2014–2024**

Pubmed: [Author and Title](#)

Google Scholar: [Author Only Title Only Author and Title](#)

**Fich EA, Segerson NA, Rose JKC (2016) The Plant Polyester Cutin: Biosynthesis, Structure, and Biological Roles. Annu Rev Plant Biol 67: 207–233**

Pubmed: [Author and Title](#)

Google Scholar: [Author Only Title Only Author and Title](#)

**Garcia H, Ferreira R, Petkovic M, Ferguson JL, Leitão MC, Gunaratne HQN, Seddon KR, Rebelo LPN, Silva Pereira C (2010) Dissolution of cork biopolymers in biocompatible ionic liquids. Green Chem 12: 367–369**

Pubmed: [Author and Title](#)

Google Scholar: [Author Only Title Only Author and Title](#)

**Garcia V, Bres C, Just D, Fernandez L, Tai FWJ, Mauxion JP, Le Paslier MC, Bérard A, Brunel D, Aoki K, et al (2016) Rapid identification of causal mutations in tomato EMS populations via mapping-by-sequencing. Nat Protoc 11: 2401–2418**

Pubmed: [Author and Title](#)

Google Scholar: [Author Only Title Only Author and Title](#)

**Girard AL, Mounet F, Lemaire-Chamley M, Gaillard C, Elmorjani K, Vivancos J, Runavot JL, Quemener B, Petit J, Germain V, et al (2012) Tomato GDSL1 is required for cutin deposition in the fruit cuticle. Plant Cell 24: 3119–3134**

Pubmed: [Author and Title](#)

Google Scholar: [Author Only Title Only Author and Title](#)

**Graça J, Lamosa P (2010) Linear and branched poly( $\omega$ -hydroxyacid) esters in plant cutins. J Agric Food Chem 58: 9666–9674**

Pubmed: [Author and Title](#)

Google Scholar: [Author Only Title Only Author and Title](#)

**Heredia-Guerrero JA, Heredia A, Domínguez E, Cingolani R, Bayer IS, Athanassiou A, Benítez JJ (2017) Cutin from agro-waste as a raw material for the production of bioplastics. J Exp Bot 68: 5401–5410**

Pubmed: [Author and Title](#)

Google Scholar: [Author Only Title Only Author and Title](#)

**Hernández Velasco BL, Arrieta-Baez D, Cortez Sotelo PI, Méndez-Méndez JV, Berdeja Martínez BM, Gómez-Patiño MB (2017) Comparative studies of cutins from lime (*Citrus aurantifolia*) and grapefruit (*Citrus paradisi*) after TFA hydrolysis. Phytochemistry 144: 78–86**

Pubmed: [Author and Title](#)

Google Scholar: [Author Only Title Only Author and Title](#)

**Ingram G, Nawrath C (2017) The roles of the cuticle in plant development: organ adhesions and beyond. J Exp Bot 68: 5307–5321**

Pubmed: [Author and Title](#)

Google Scholar: [Author Only Title Only Author and Title](#)

**Just D, Garcia V, Fernandez L, Bres C, Mauxion J-P, Petit J, Jorly J, Assali J, Bournonville C, Ferrand C, et al (2013) Micro-Tom mutants for functional analysis of target genes and discovery of new alleles in tomato. Plant Biotechnol 30: 225–231**

Pubmed: [Author and Title](#)

Google Scholar: [Author Only Title Only Author and Title](#)

**Li Y, Wang J, Liu X, Zhang S (2018) Towards a molecular understanding of cellulose dissolution in ionic liquids: Anion/cation effect, synergistic mechanism and physicochemical aspects. Chem Sci 9: 4027–4043**

Pubmed: [Author and Title](#)

Google Scholar: [Author Only Title Only Author and Title](#)

**Lyerla JR (1980) High-resolution nuclear magnetic resonance spectroscopy. Methods Exp Phys 16: 241–369**

Pubmed: [Author and Title](#)

Google Scholar: [Author Only Title Only Author and Title](#)

**Matas AJ, Yeats TH, Buda GJ, Zheng Y, Chatterjee S, Tohge T, Ponnala L, Adato A, Aharoni A, Stark R, et al (2011) Tissue- and cell-type specific transcriptome profiling of expanding tomato fruit provides insights into metabolic and regulatory specialization and cuticle formation. Plant Cell 23: 3893–3910**

Pubmed: [Author and Title](#)

Google Scholar: [Author Only Title Only Author and Title](#)

**Mazurek S, Garroum I, Daraspe J, Bellis D De, Olsson V, Mucciolo A, Butenko MA, Humbel BM, Nawrath C (2017) Connecting the Molecular Structure of Cutin to Ultrastructure and Physical Properties of the Cuticle in Petals of Arabidopsis. Plant Physiol 173: 1146–1163**

Pubmed: [Author and Title](#)

Google Scholar: [Author Only Title Only Author and Title](#)

**Mykhaylyk OO, Smith KW, Martin CM, Ryan AJ (2007) Structural models of metastable phases occurring during the crystallization process of saturated/unsaturated triacylglycerols. J Appl Crystallogr 40: s297–s302**

Pubmed: [Author and Title](#)

Google Scholar: [Author Only Title Only Author and Title](#)

**Nawrath C, Schreiber L, Franke RB, Geldner N, Reina-Pinto JJ, Kunst L (2013) Apoplastic Diffusion Barriers in Arabidopsis. Arab B. doi: 10.1199/tab.0167**

Pubmed: [Author and Title](#)

Google Scholar: [Author Only Title Only Author and Title](#)

**Petit J, Bres C, Mauxion J-P, Bakan B, Rothan C (2017) Breeding for cuticle-associated traits in crop species: traits, targets, and strategies. J Exp Bot 68: 5369–5387**

Pubmed: [Author and Title](#)

Google Scholar: [Author Only Title Only Author and Title](#)

**Petit J, Bres C, Mauxion JP, Tai FWJ, Martin LBB, Fich EA, Joubès J, Rose JKC, Domergue F, Rothan C (2016) The glycerol-3-phosphate acyltransferase GPAT6 from tomato plays a central role in fruit cutin biosynthesis. Plant Physiol 171: 894–913**

Pubmed: [Author and Title](#)

Google Scholar: [Author Only Title Only Author and Title](#)

**Petkovic M, Ferguson JL, Gunaratne HQN, Ferreira R, Leitão MC, Seddon KR, Rebelo LPN, Silva Pereira C (2010) Novel biocompatible cholinium-based ionic liquids - Toxicity and biodegradability. Green Chem 12: 643–649**

Pubmed: [Author and Title](#)

Google Scholar: [Author Only Title Only Author and Title](#)

**Philippe G, Gaillard C, Petit J, Geneix N, Dalgarrondo M, Bres C, Mauxion J-P, Franke R, Rothan C, Schreiber L, et al (2016) Ester Cross-Link Profiling of the Cutin Polymer of Wild-Type and Cutin Synthase Tomato Mutants Highlights Different Mechanisms of Polymerization. Plant Physiol 170: 807–820**

Pubmed: [Author and Title](#)

Google Scholar: [Author Only Title Only Author and Title](#)

**Philippe G, Geneix N, Petit J, Guillon F, Sandt C, Rothan C, Lahaye M, Marion D, Bakan B (2020) Plant cuticle embedded polysaccharides exhibit specific structural features. New Phytol (in press)**

Pubmed: [Author and Title](#)

Google Scholar: [Author Only Title Only Author and Title](#)

**Rogers RD, Seddon KR (2003) Ionic Liquids - Solvents of the Future? Science 302: 792–793**

**Rongpipi S, Ye D, Gomez ED, Gomez EW (2019) Progress and opportunities in the characterization of cellulose – an important regulator of cell wall growth and mechanics. Front Plant Sci 9: 1894**

Pubmed: [Author and Title](#)

Google Scholar: [Author Only Title Only Author and Title](#)

**Rothan C, Just D, Fernandez L, Aienza I, Ballias P, Lemaire-Chamley M (2016) Culture of the tomato Micro-Tom Cultivar in greenhouse. Methods Mol. Biol. Humana Press Inc., pp 57–64**

Pubmed: [Author and Title](#)

Google Scholar: [Author Only Title Only Author and Title](#)

**Segado P, Domínguez E, Heredia A (2016) Ultrastructure of the Epidermal Cell Wall and Cuticle of Tomato Fruit ( *Solanum lycopersicum* L.) during Development. Plant Physiol 170: 935–946**

Pubmed: [Author and Title](#)

Google Scholar: [Author Only Title Only Author and Title](#)

**Small DM (1984) Lateral chain packing in lipids and membranes. J Lipid Res 25: 1490–1500**

Pubmed: [Author and Title](#)

Google Scholar: [Author Only Title Only Author and Title](#)

**Southern JH, Weeks N, Porter RS, Crystal RG (1972) Unique polyethylene morphologies produced under extrusion conditions. Macromol Chem Phys 162: 19–30**

Pubmed: [Author and Title](#)

Google Scholar: [Author Only Title Only Author and Title](#)

**Yeats TH, Huang W, Chatterjee S, Viart HMF, Clausen MH, Stark RE, Rose JKC (2014) Tomato Cutin Deficient 1 (CD1) and putative orthologs comprise an ancient family of cutin synthase-like (CUS) proteins that are conserved among land plants. Plant J 77: 667–675**

Pubmed: [Author and Title](#)

Google Scholar: [Author Only Title Only Author and Title](#)

**Yeats TH, Martin LBB, Viart HMF, Isaacson T, He Y, Zhao L, Matas AJ, Buda GJ, Domozych DS, Clausen MH, et al (2012) The identification of cutin synthase: Formation of the plant polyester cutin. Nat Chem Biol 8: 609–611**

Pubmed: [Author and Title](#)

Google Scholar: [Author Only Title Only Author and Title](#)

**Zhang X, Zhang A, Liu C, Ren J (2016) Per-O-acylation of xylan at room temperature in dimethylsulfoxide/N-methylimidazole. Cellulose 23: 2863–2876**

Pubmed: [Author and Title](#)

Google Scholar: [Author Only Title Only Author and Title](#)